2007

# Neoplasia driven by mutant c-KIT Is mediated by intracellular, not plasma membrane, receptor signaling

Zhifu Xiang
*Washington University School of Medicine in St. Louis*
Frederike Kreisel
*Washington University School of Medicine in St. Louis*
Jennifer Cain
*Washington University School of Medicine in St. Louis*
AnnaLynn Colson
*Washington University School of Medicine in St. Louis*
Michael H. Tomasson
*Washington University School of Medicine in St. Louis*

Molecular and Cellular Biology

# Neoplasia Driven by Mutant c-*KIT* Is Mediated by Intracellular, Not Plasma Membrane, Receptor Signaling

**Zhifu Xiang, Frederike Kreisel, Jennifer Cain, AnnaLynn Colson and Michael H. Tomasson**

***Mol. Cell. Biol.*** **2007, 27(1):267. DOI: 10.1128/MCB.01153-06.**
**Published Ahead of Print 23 October 2006.**

MOLECULAR AND CELLULAR BIOLOGY, Jan. 2007, p. 267–282 Vol. 27, No. 1
0270-7306/07/$08.00+0 doi:10.1128/MCB.01153-06


# Neoplasia Driven by Mutant c-*KIT* Is Mediated by Intracellular, Not Plasma Membrane, Receptor Signaling▽

Zhifu Xiang,[1] Frederike Kreisel,[2] Jennifer Cain,[1] AnnaLynn Colson,[1] and Michael H. Tomasson[1]*

*Department of Internal Medicine, Division of Oncology,[1] and Department of Pathology,[2] Washington University School of Medicine, Siteman Cancer Center, St. Louis, Missouri 63110*

Received 27 June 2006/Returned for modification 26 July 2006/Accepted 9 October 2006

**Activating mutations in *c-KIT* are associated with gastrointestinal stromal tumors, mastocytosis, and acute myeloid leukemia. In attempting to establish a murine model of human $KIT^{D816V}$ ($hKIT^{D816V}$)-mediated leukemia, we uncovered an unexpected relationship between cellular transformation and intracellular trafficking. We found that transport of $hKIT^{D816V}$ protein was blocked at the endoplasmic reticulum in a species-specific fashion. We exploited these species-specific trafficking differences and a set of localization domain-tagged *KIT* mutants to explore the relationship between subcellular localization of mutant KIT and cellular transformation. The protein products of fully transforming *KIT* mutants localized to the Golgi apparatus and to a lesser extent the plasma membrane. Domain-tagged $KIT^{D816V}$ targeted to the Golgi apparatus remained constitutively active and transforming. Chemical inhibition of intracellular transport demonstrated that Golgi localization is sufficient, but plasma membrane localization is dispensable, for downstream signaling mediated by KIT mutation. When expressed in murine bone marrow, endoplasmic reticulum-localized $hKIT^{D816V}$ failed to induce disease in mice, while expression of either Golgi-localized $HyKIT^{D816V}$ or cytosol-localized, ectodomain-deleted $KIT^{D816V}$ uniformly caused fatal myeloproliferative diseases. Taken together, these data demonstrate that intracellular, non-plasma membrane receptor signaling is sufficient to drive neoplasia caused by mutant c-*KIT* and provide the first animal model of myelomonocytic neoplasia initiated by human $KIT^{D816V}$.**

The c-*Kit* gene is the mammalian homolog of the Hardy-Zuckerman 4 feline sarcoma virus-transforming sequence (5), maps to the murine *white spotted* (*W*) locus (12), and encodes a type III receptor tyrosine kinase (RTK) (26, 31) sharing strong sequence similarity to other type III RTK members FLT3, FMS, and platelet-derived growth factor receptor (32). The KIT receptor is expressed in hematopoietic stem cells, mast cells, neural crest-derived melanocytes, and germ cells. Immunoprecipitation studies of Kit expression demonstrated two protein products, 160 kDa and 140 kDa, detectable in Kit-expressing cells due to different posttranslational glycosylation (32). Binding to KIT ligand (stem cell factor [SCF]) leads to receptor dimerization, activation of the intrinsic receptor kinase, and initiation of a spectrum of downstream signaling cascades responsible for various cellular responses, such as proliferation, migration, and survival (7).

Gain-of-function mutations in c-*KIT*, causing constitutive, ligand-independent activation of the receptor, were first identified in neoplastic mast cell lines of human, mouse, and rat origins (11, 36, 37). Activating mutations in the human c-*KIT* gene (*KIT*) occur in association with systemic mastocytosis (24), gastrointestinal stromal tumors (33), germ cell tumors (29), and acute myeloid leukemia (AML) (1, 15). Among these mutations, D816V is the most frequent mutation. The wild-type KIT receptor is widely expressed in the blast cells of AML. *KIT* mutations in unselected AML cases occur only in 2% of cases, but occur at a high frequency in certain AML subtypes, i.e., in about 48% of core binding factor leukemias (2, 3, 38). In erythroleukemia developed in spi-1/PU.1 transgenic mice, acquired Kit mutations occur in 86% of tumors (19). The $KIT^{D816V}$ mutation is predicted to cause ligand-independent receptor activation by disrupting the structure of the tyrosine kinase domain activation loop (10). Expression of human $KIT^{D816V}$ ($hKIT^{D816V}$) has been reported to transform Myb-immortalized murine cells (10), but an animal model using primary hematopoietic cells expressing the human $KIT^{D816V}$ mutation has not been reported. Expression of the homologous murine Kit mutation, encoding an identical aspartic acid-to-valine substitution ($Kit^{D814V}$), induces factor-independent growth of hematopoietic cell lines (17), transforms normal hematopoietic cells (18), and induces lymphoid malignancies in mice (18). Studies on FLT3 internal tandem duplication (FLT3 ITD) demonstrate that FLT3 activation induces significantly reduced surface expression and increased accumulation of immature protein in subcellular compartments, suggesting that constitutive phosphorylation of the FLT3 receptor impairs its posttranslational processing and trafficking (34); however, the mechanisms contributing to this phenomenon remain to be elucidated. Furthermore, it is known that accumulated, immature KIT protein and other RTK receptors (i.e., FLT3 ITD) can be phosphorylated (9, 34); however, it is unclear whether phosphorylation of those non-membrane-localized receptors is also biologically active and contributes to tumorigenesis in vivo.

We sought to develop a mouse model of $hKIT^{D816V}$-induced disease as a platform to dissect the molecular mechanisms underlying RTK contributions to myeloid leukemia development. To our surprise, murine cells were repeatedly and inex-

* Corresponding author. Mailing address: Washington University School of Medicine, Campus Box 8007, 660 South Euclid Avenue, St. Louis, MO 63110. Phone: (314) 362-9350. Fax: (314) 362-9333. E-mail: tomasson@wustl.edu.

▽ Published ahead of print on 23 October 2006.

plicably resistant to transformation by *hKIT*$^{D816V}$. Noting that murine and human KIT extracellular domains are not structurally identical, we hypothesized that the human KIT extracellular domain was inhibiting proper protein expression and preventing transformation of murine cells. While the C-terminal intracellular signaling domains of the murine Kit and human KIT proteins are 93% homologous at the amino acid level, the extracellular domains of mouse Kit and human KIT share only 74% homology and have significant functional structural differences. Specifically, the ligand binding domains of the human KIT receptor lie in the second immunoglobulin (Ig)-like domain, while the binding site of the murine ligand lies in an adjacent but noncontiguous region (20) and, correspondingly, the murine and human KIT receptors do not possess identical ligand binding capabilities. To facilitate mutant KIT receptor expression and transformation, we engineered novel chimeric receptors (HyKIT$^{WT}$ and HyKIT$^{D816V}$) by fusing the extracellular and transmembrane domains of the murine *Kit* in frame to the intracellular signaling domain of human *KIT*. We compared the transformation potential of the murine, human, and hybrid mutants by expressing *hKIT*$^{D816V}$, *mKit*$^{D814V}$, and *HyKIT*$^{D816V}$ in cell lines of both murine and human origins. We examined the expression and subcellular localization of the encoded proteins using Western blotting, flow cytometry, endoglycosidase digestion, and immunofluorescence microscopy. We examined the downstream signaling pathways activated by these KIT mutants and tested their ability to induce leukemia in murine bone marrow transduction/transplantation assays. The results of intracellular localization, signaling, and transformation experiments all supported the model that *hKIT*$^{D816V}$ is trapped by an endoplasmic reticulum (ER) checkpoint, specifically in murine cells, that can recognize differences between homologous human and murine mutant glycoproteins. The *HyKIT*$^{D816V}$ receptor overcame this checkpoint block and uniformly induced fatal myeloproliferative disease (MPD) in mice, demonstrating a unique and useful model of KIT-induced myeloid disease. Furthermore, by artificially targeting KIT expression to the Golgi apparatus, KIT D816V retained its constitutive activation and transformation potential; treatment with chemical inhibitors of intracellular transport suggested that Golgi compartment localization was sufficient for downstream signaling pathway activation mediated by KIT mutation. Taken together, these data provide strong evidence that the signaling activated by intracellularly localized KIT receptor plays an important role in mutant *KIT*-mediated transformation and tumorigenesis.

## MATERIALS AND METHODS

**Plasmid DNA constructs.** pRUFNeo plasmids containing the whole coding sequence of wild-type human *KIT* cDNA and activating mutant (816 Asp→Val; D816V) human *KIT* cDNA were generously provided by Leonie Ashman (Hanson Centre for Cancer Research, Adelaide, Australia). Two steps were used to introduce both wild-type and mutant human c-*KIT* cDNA from pRUFNeo into retroviral vector *MSCV-IRES-eGFP* (*MIG*): first, a BamHI-BglII upstream fragment was ligated to the BglII site of *MIG*, and after orientation confirmation, the downstream BglII-BglII fragment was introduced to create whole coding region of the human c-*KIT* gene. The resulting constructs were named *MIG-hKIT*$^{WT}$ and *MIG-hKIT*$^{D816V}$, respectively. To create *MIG-mKit*$^{D814V}$, murine *Kit* cDNA containing the D814V mutation (kind gift from M. Mizuki, Osaka University Graduate School of Medicine, Japan) was subcloned into the EcoRI site of *MIG*.

To generate murine-human hybrid *KIT* cDNA, the extracellular region and transmembrane region of murine c-*Kit* cDNA were fused in frame with the intracellular region of human c-*KIT* cDNA containing either the wild type or D816V mutant. The resulting constructs were named *MIG-HyKIT*$^{WT}$ and *MIG-HyKIT*$^{D816V}$, respectively.

In order to target KIT intracellular domain expression to the cell membrane, a fusion sequence consisting of the N-terminal 20 amino acids of neuromodulin, also called *GAP-43*, and the entire c-*KIT* intracellular domain (ICD) was generated in frame by PCR and three-way ligation. The neuromodulin fragment (*GAP-43*), which contains a signal for posttranslational palmitoylation of cysteines 3 and 4 (41), was synthesized by Integrated DNA Technologies Inc. (Coralville, IA) with a BglII restriction site added to its 5′ end and a NcoI site added to its 3′ end. *KIT ICD* fragments were amplified from *MIG-hKIT*$^{WT}$ and *MIG-hKIT*$^{D816V}$ plasmids, respectively, using the Expand high-fidelity PCR system (Roche Applied Science, Mannheim, Germany) with the following primers: forward primer with NcoI restriction site, 5′-CGCCCATGGCTGACCTACAA ATATTTACAGAAACCC; reverse primer with EcoRI restriction site, 5′-GGA GAATTCAGACATCGTCGTGCACAAG. The *GAP-43* fragment and *KIT ICD* fragment were digested with appropriate restriction enzymes and subcloned into the *MIG* retroviral vector, and resulting constructs were named *MIG-GAP-KIT*$^{WT}$ and *MIG-GAP-KIT*$^{D816V}$, respectively.

In order to target expression of the KIT intracellular domain specifically to the Golgi apparatus, an in-frame fusion of *FIG* (*f*used *i*n *g*lioblastoma), a gene coding for a Golgi apparatus-associated protein (8), to *KIT ICD* was generated in a similar way as described above. A *FIG-ROS* cDNA, a kind gift from A. Charest (MIT Center for Cancer Research, Cambridge, MA), was used as the template to amplify the *FIG* fragment using the following primers: forward primer with BglII restriction site, 5′-AGTAAGATCTATGTCGGCGGGCGGT CCATG; reverse primer with NcoI restriction site, 5′-CCGCCCATGGTTGTA ATACTTTGATTTCCC. The *KIT ICD* fragment was amplified as described above. Both the *FIG* fragment and *KIT ICD* fragment were digested with appropriate restriction enzymes and subcloned into the *MIG* retroviral vector, and resulting constructs were named *MIG-FIG-KIT*$^{WT}$ and *MIG-FIG-KIT*$^{D816V}$, respectively. Ninety percent of FIG sequence, including the two coiled-coil motifs and the PDZ domain, are retained in the FIG-KIT fusion protein.

To express only the KIT intracellular domain, the *KIT ICD* fragment was amplified from *MIG-hKIT*$^{WT}$ and *MIG-hKIT*$^{D816V}$ plasmids, respectively. A BglII restriction site and start codon ATG were added to the forward primer, 5′-CG CAGATCTATGCTGACCTACAAATATTTACAGA AACCC. 3′ primer sequence was as described above. The PCR product was digested with BglII and EcoRI and subcloned into the *MIG* retroviral vector. The constructs were named *MIG-ICD-KIT*$^{WT}$ and MIG-*ICD-KIT*$^{D816V}$, respectively.

The sequences of all constructs used in this study were verified by restriction mapping and direct sequencing. All plasmids were prepared by double cesium-banding purification.

**Cell Culture.** 293T cells, NIH 3T3 cells, and A375 cells were grown in Dulbecco's modified Eagle's medium (Cambrex Bio Science Walkersville Inc., Walkersville, MD) containing 10% fetal calf serum (FCS; HyClone, Logan UT) and 1× penicillin-streptomycin (Pen/Strep) in a humidified incubator at 37°C, 5% $CO_2$. Cytokine-dependent Ba/F3 murine hematopoietic cells and TF-1 human hematopoietic cells were maintained in RPMI 1640 (Cambrex Bio Science Walkersville Inc., Walkersville, MD) supplemented with 10% FCS, 1× Pen/Strep, and 1 ng/ml of either recombinant mouse interleukin-3 (rmIL-3; R&D Systems Inc., Minneapolis, MN) or rhIL3 (STEMCELL Technologies Inc., Vancouver, British Columbia, Canada), respectively. K562 cells were grown in RPMI containing 10% FCS and 1× Pen/Strep. Primary murine bone marrow mononuclear cells were plated in transplant medium consisting of RPMI 1640, 20% FCS, and 1× Pen/Strep with 10 ng/ml SCF, 6 ng/ml IL-3, 50 ng/ml Flt-3 (R&D Systems Inc.), and 10 ng/ml thrombopoietin (PeproTech, Rocky Hill, NJ).

**Retroviral production.** Ecotropic retrovirus used to transduce murine cells was generated by transient transfection of 293T cells as described previously (13). Amphotropic retrovirus used to transduce human cells was generated by transient cotransfection of 293T cells with retroviral construct and packaging plasmids pMD.G and pMD.Gagpol. Viral supernatant was harvested 48 h posttransfection, and the titer of the infectious virus was determined by flow cytometry using NIH 3T3 cells infected with serial dilutions of virus in the presence of 10 μg/ml of Polybrene (American Bioanalytical, Natick, MA).

**Cell growth and proliferation assays.** Murine cell line Ba/F3 cells or human cell line TF-1 cells transduced with retroviruses were sorted by MoFlo (DAKO/Cytomation) based on equivalent green fluorescent protein (GFP) expression levels. Sorted cells were recovered with the appropriate growth medium as described above and washed with RPMI 1640 thrice to remove growth factor (IL-3) and resuspended with RPMI 1640 containing 10% FCS and 1× Pen/Strep. Cells were plated into either 12-well plates or 96-well plates in the absence of IL-3. Viable cells were counted daily by staining with trypan blue or evaluated by

thiazolyl blue tetrazolium bromide (MTT) assay using the CellTiter 96 Aqueous One Solution cell proliferation assay kit (Promega, Madison, WI).

**Immunofluorescence staining.** Cells growing on glass coverslips were transfected with c-Kit MIG expression plasmids using SuperFect reagent (QIAGEN, Valencia, CA) and fixed with 3.7% formaldehyde (Sigma-Aldrich, St. Louis, MO) in phosphate-buffered saline (PBS) for 15 min at room temperature. After three washes with PBS for 5 min each, cells were incubated with primary antibody with gentle agitation at room temperature for 1 h. Primary antibodies were visualized by subsequent staining with secondary antibodies conjugated to either Alexa Fluor 350, Alexa Fluor 594, or Alexa Fluor 633 (Molecular Probes Inc., Eugene, OR). Goat anti-c-Kit antibody (clone C-14; Santa Cruz Biotechnology, Santa Cruz, CA) was used for detection of c-Kit protein. Golgi complex and endoplasmic reticulum were stained with rabbit anti-GPP130 antibody (Covance Research Products, Berkeley, CA) or rabbit anti-calnexin antibody (Sigma-Aldrich, St. Louis MO), respectively. All antibodies were diluted in PBS containing 1 mg/ml bovine serum albumin, 0.2% Triton X-100, and 5% FCS. Images were taken with a Zeiss LSM510 laser-scanning confocal microscope.

**Semiquantitative RT-PCR.** Total RNA was isolated from transduced and sorted Ba/F3 cells using TRIzol reagent (Invitrogen, Carlsbad, CA). Reverse transcription (RT) was performed with Superscript III (Invitrogen). PCR cycles (18, 22, 26, and 30 cycles) were performed using the following primers: glyceraldehyde-3-phosphate dehydrogenase forward, 5′-TGCAGTGGCAAAGTGGAGATT, and reverse, 5′-TTGAAGTCGCAGGAGACAACCT; c-Kit forward primer, 5′-GGCAGCCAGAAATATCCTCCTTAC, and reverse primer, 5′-CACGGGCTTCTGTCGGTTGG.

**Immunoblotting and immunoprecipitation.** Cells were transduced with the KIT allele and sorted based on equivalent GFP expression levels. Cells were lysed in an appropriate amount of RIPA lysis buffer (50 mM Tris-HCl, pH 7.4, 150 mM sodium chloride, 0.25% deoxycholic acid, 1% NP-40, 1 mM EDTA) supplemented with 1 mM $Na_3VO_4$, 25 mM NaF, 1 mM phenylmethylsulfonyl fluoride, and 1× Complete protease inhibitor cocktail (Roche, Indianapolis, IN). Lysates were incubated for 15 min on ice and then cleared by centrifugation at 14,000 × *g* for 15 min at 4°C. Freshly prepared lysates were used for all immunoprecipitations. Immunoprecipitations were performed by incubating 500 to 1,000 μg total cell lysate on a rocker at 4°C for 2 h with polyclonal goat anti-c-Kit antibody (C-14). Immunoprecipitates were collected with protein G-Sepharose (Amersham-Pharmacia Biotech, Piscataway, NJ). Immunoprecipitates were washed three times with lysis buffer and boiled for 5 min in sodium dodecyl sulfate (SDS) sample buffer. Immunoblotting was performed following a standard protocol. Briefly, samples were separated by SDS-polyacrylamide gel electrophoresis (SDS-PAGE) and transferred electrophoretically to nitrocellulose membrane (Schleicher & Schuell BioScience, Keene, NH). Blot was blocked with 5% dry milk in Tris-buffered saline-Tween 20 buffer and then incubated overnight at 4°C with one of the following antibodies: goat anti-c-kit (C-14), rabbit anti-phospho-c-kit (Tyr719; Cell Signaling Technology, Beverly, MA), mouse anti-Akt and mouse anti-phospho-Akt, rabbit anti-p44/42 mitogen-activated protein kinase (MAPK) and rabbit anti-phospho-p44/42 MAPK (Cell Signaling), rabbit anti-Stat3 and rabbit anti-phospho-Stat3 (Cell Signaling), rabbit anti-Stat5 and rabbit anti-phospho-Stat5 (Cell Signaling), rabbit anti-phospho-(Tyr) p85 phosphatidyl inositol 3-kinase (PI3K) binding motif antibody (Cell Signaling), and mouse anti-β-actin (Sigma, St. Louis, MO). Blots were incubated with horseradish peroxidase-conjugated secondary antibodies (Amersham Biosciences Corp., Piscataway, NJ) and visualized by enhanced chemiluminescence (Pierce Biotechnology, Rockford, IL).

**Glycosidase treatment.** Whole-cell lysates were treated with either peptide *N*-glycosidase (PNGase F) or endo-β-*N*-acetylglucosaminidase H (Endo H) (both from New England Biolabs, Ipswich, MA) for at least 2 h at 37°C per the manufacturer's instructions. The reactions were terminated with SDS-PAGE sample buffer, and the reaction product was analyzed by immunoblotting as described above.

**Murine bone marrow transplantation.** BALB/c female mice (6 to 8 weeks of age) were purchased from Taconic Farms and maintained in an accredited animal facility according to proper institutional guidelines. Retroviral transduction and transplantation of bone marrow cells were carried out as described previously (35). Briefly, bone marrow mononuclear cells were isolated from the femurs and tibias of donor mice pretreated with a single dose 5-fluorouracil (150 mg/kg of body weight) for 2 days. After 48 h of culture in transplant medium, bone marrow cells were transduced by two rounds of spin-infection with equivalent titer of retroviral stocks. Syngeneic recipient mice irradiated with 900 cGy were transplanted intravenously with $1 \times 10^6$ unfractionated transduced bone marrow cells. Samples were collected from moribund mice as described previously (13). Kaplan-Meier plots were generated on groups of mice on the basis of cumulative survival after transplantation using STATVIEW software (SAS Institute, Cary, NC). Cell morphology was performed on slides prepared from peripheral blood (PB), bone marrow (BM), and spleen (SP) cells from sick mice by May-Grünwald/Giemsa staining and imaged as described elsewhere (25).

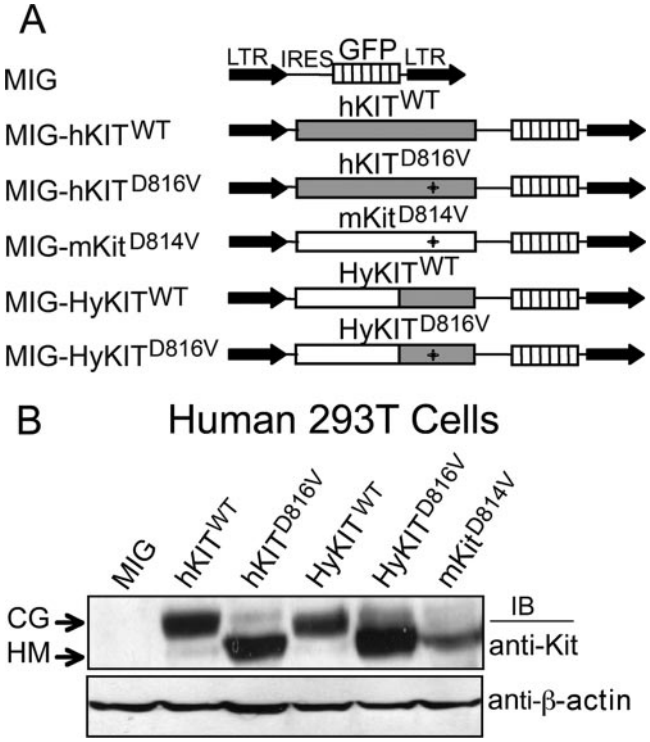


FIG. 1. Schematic diagram of *KIT* allele constructs and analysis of protein expression in 293T cells. (A) Schematic diagram of wild-type and mutant *KIT* constructs. Retroviral constructs were generated by subcloning wild-type human *KIT* (*hKIT$^{WT}$*) cDNA and human *KIT* cDNA containing a point mutation encoding an aspartic acid→valine substitution at position 816 in the cytoplasmic activation loop of KIT (*hKIT$^{D816V}$*) into the *MSCV-IRES-GFP* retroviral vector (MIG). Murine-human hybrid *KIT* alleles (*HyKIT$^{WT}$* and *HyKIT$^{D816V}$*) were generated by fusing in frame the extracellular/transmembrane domains of murine *Kit* to the cytoplasmic domains of human *KIT*. The murine *Kit* cDNA containing a mutation encoding the identical amino acid substitution at the identical conserved activation loop aspartic acid residue (*mKit$^{D814V}$*) was used as a control. Human sequences are indicated by shaded boxes, and the murine sequence is indicated by open boxes. The plus symbol indicates mutation in the cytoplasmic domain. (B) All *KIT* allele constructs express transgene protein appropriately in human 293T cells. Whole-cell protein lysates from transient-transfected human 293T cells were analyzed by immunoblotting with antibody to c-Kit recognizing intracellular domain of both human c-KIT and murine c-Kit proteins. Faster migration of mutant proteins was confirmed in subsequent experiments (described in the text) to be due to differential glycosylation patterns. CG, complex glycosylation form; HM, high-mannose (immature) form.

**Flow cytometry.** Flow cytometry was performed as described previously (13). The antibodies used to detect the murine antigens were Gr-1, CD11b, CD117 (c-Kit), Sca-1, B220, CD43, IgM, CD3, CD4, CD8, and Ter-119. All antibodies were purchased from BD PharMingen (San Jose, CA). Analysis was performed on 7-aminoactinomycin D-negative cells by using FLOWJO software (Tree Star, San Carlos, CA). Quadrants were set on the basis of isotype control antibodies conjugated to phycoerythrin or peridinin chlorophyll *a* protein.

## RESULTS

**Human but not murine cells are rapidly transformed by expression of human *KIT$^{D816V}$*.** The *KIT$^{D816V}$* mutation is the

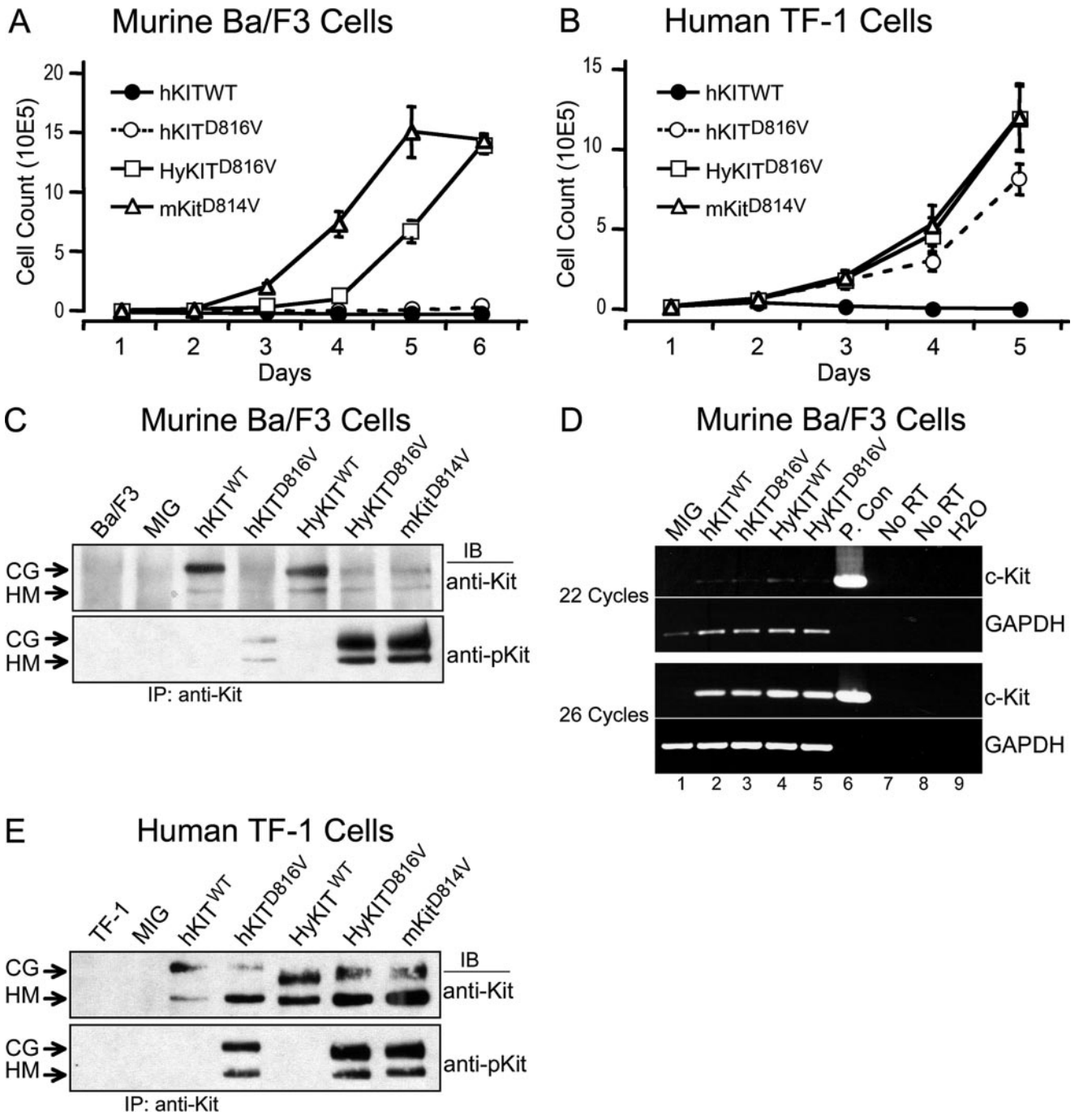


FIG. 2. Cellular transformation by mutant *hKIT*$^{D816V}$ is blocked in murine cells by posttranscriptional inhibition of protein expression and is restored by murine extracellular/transmembrane sequences. (A) Transformation of murine Ba/F3 cells to cytokine-independent growth by *KIT* alleles. Ba/F3 cells expressing different *KIT* alleles were starved of IL-3, and viable cells were counted daily by trypan blue exclusion. Cells expressing *HyKIT*$^{D816V}$ and *mKit*$^{D814V}$ grew rapidly following IL-3 withdrawal, but *hKIT*$^{D816V}$-expressing cells failed to grow after 1 week. After an additional week in culture, a subpopulation of *hKIT*$^{D816V}$-expressing cells grew in the absence of IL-3 (not shown). Mock-infected, vector-alone, and *HyKIT*$^{WT}$ control cell populations did not grow in the absence of IL-3 (same growth pattern as *hKIT*$^{WT}$) (data not shown). (B) Transformation of human TF-1 cells to cytokine-independent growth by *KIT* alleles. TF-1 cells expressing different *KIT* alleles were starved of IL-3, and viable cells were counted daily. Human cells expressing *hKIT*$^{D816V}$ (as well as *HyKIT*$^{D816V}$ and *mKit*$^{D814V}$) grew in the absence of IL-3 without prolonged selection. (C) Expression and autophosphorylation of KIT receptor proteins in murine Ba/F3 cells. Total cell lysates were prepared from Ba/F3 cells expressing different *KIT* alleles, immunoprecipitated with anti-c-Kit antibody, and blotted with either anti-Kit antibody or with phospho-specific anti-Kit antibody. Expression of hKIT$^{D816V}$ protein was significantly inhibited compared to HyKIT$^{D816V}$ and mKit$^{D814V}$ proteins. CG, complex glycosylated form; HM, high-mannose (immature) form. (D) Semiquantitative RT-PCR demonstrated equivalent expression of all KIT receptor alleles in Ba/F3 cells at the RNA level. Total RNA was isolated from transduced and sorted GFP-positive Ba/F3 cells from each construct, and an equal amount of total RNA was used as template in RT-PCR with oligo(dT) primers for cDNA synthesis and gene-specific primers as indicated. PCR was carried out with 18, 22, 26, and 30 amplification cycles for linear range determination. Data from 22 and 26 cycles of PCR are shown here. Lanes 1 to 5, cDNA from different *KIT* alleles as indicated; lane 6, positive control using *MIG-hKIT*$^{WT}$ plasmid, 20 ng per reaction mixture; lanes 7 and 8, no RT control of RNA samples from *hKIT*$^{WT}$- and *hKIT*$^{D816V}$-transduced Ba/F3 cells, respectively; lane 9, no-template water control. (E) Expression and autophosphorylation of KIT receptor proteins in human TF-1 cells. Immunoprecipitation and immunoblotting were carried out as for panel C. In human cells, expression of mutant KIT receptor proteins, including hKIT$^{D816V}$, achieved equivalent levels of protein expression.

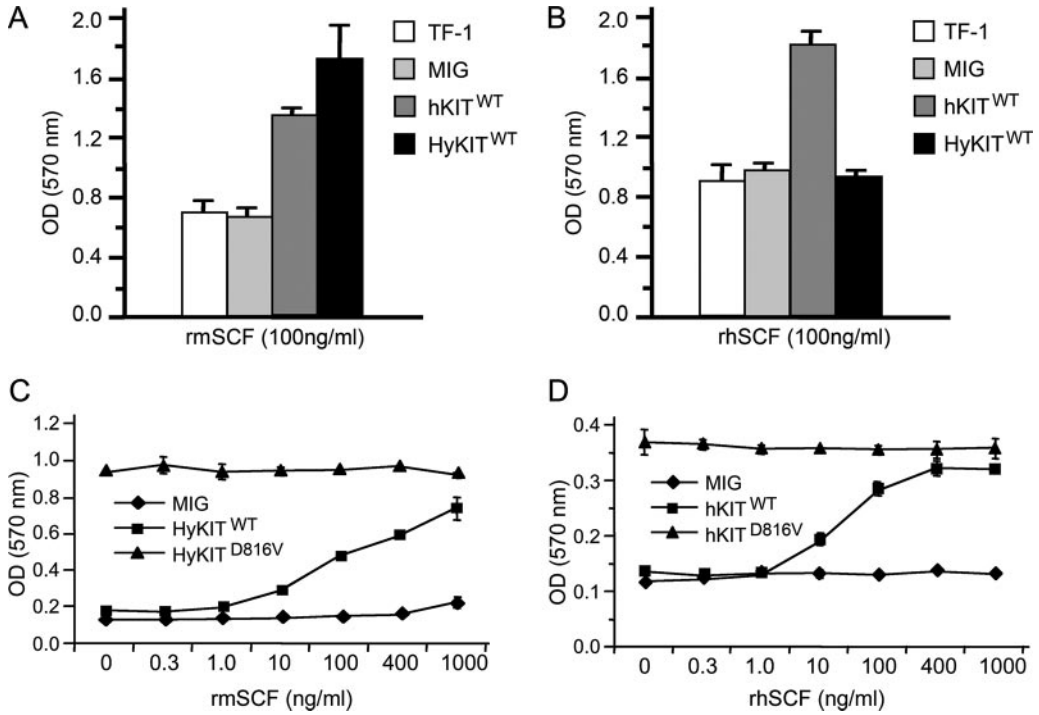


FIG. 3. KIT$^{D816V}$ receptors induce ligand-independent growth. (A) Murine ligand stimulates growth of TF-1 cells expressing *hKIT$^{WT}$* and *HyKIT$^{WT}$*. Parental and transduced TF-1 cells were washed three times with RPMI 1640 to remove IL-3 and restimulated with 100 ng/ml rmSCF. At 48 h after restimulation, cell proliferation was measured by MTT assay. (B) Human ligand only stimulates growth of TF-1 cells expressing *hKIT$^{WT}$* but not *HyKIT$^{WT}$*. (C) Cells expressing *HyKIT$^{D816V}$* are insensitive to Kit ligand. Transduced Ba/F3 cells were washed three times to remove IL-3 and restimulated with rmSCF with various dosages. Cell proliferation was measured by MTT assay. Cells expressing *HyKIT$^{WT}$* responded to rmSCF in a dose-dependent manner, while cells expressing *HyKIT$^{D816V}$* grew in a dose-independent manner. (D) Cells expressing *hKIT$^{D816V}$* are insensitive to KIT ligand. Ba/F3 cells expressing *hKIT$^{D816V}$* were starved of IL-3 for 1 week, and then prestarved *hKIT$^{D816V}$* cells were used for MTT assay as described above.

most common gain-of-function c-*KIT* mutation associated with human diseases and is predicted to cause ligand-independent receptor activation (24, 29, 33, 38). To test its transforming potential in vitro and in vivo, we generated retroviral constructs expressing mutant KIT D816V (hKIT$^{D816V}$) along with the homologous murine mutant Kit D814V (*mKit$^{D814V}$*) (Fig. 1A) and validated their expression in transfected human 293T cells by Western blotting (Fig. 1B). We assessed the ability of these *KIT* alleles to transform murine IL-3-dependent Ba/F3 cells to growth factor independence. Surprisingly, homologous mutant *KIT* alleles displayed significant differences in transformation potential (Fig. 2A). The fully murine *mKit$^{D814V}$* caused the most rapid outgrowth of cells in the absence of IL-3 but, notably, we found that the *hKIT$^{D816V}$* failed to transform murine Ba/F3 cells in this short-term growth assay. This unexpected finding promoted us to wonder if *hKIT$^{D816V}$* could transform cells from different cell lineages or origins, and we repeated the experiments by expressing *hKIT$^{D816V}$* in both murine 32D myeloid leukemia cells and human TF-1 erythroid leukemia cells. In agreement with Ba/F3 data, *hKIT$^{D816V}$* could not transform murine 32D cells (data not shown). In contrast to the poor transformation potential of *hKIT$^{D816V}$* in murine cells, *hKIT$^{D816V}$* could rapidly transform human TF-1 cells to cytokine independence (Fig. 2B). We examined RNA expression of *hKIT$^{D816V}$* in these cells and found equivalent transcript levels (Fig. 2D), but levels of the hKIT$^{D816V}$ protein were specifically reduced in murine Ba/F3 cells (Fig. 2C) in comparison to human cells (Fig. 1B and 2E). Reduced protein expression of hKIT$^{D816V}$ was also observed in murine 3T3 and 32D cells (data not shown), but robust hKIT$^{D816V}$ expression was observed in all human cell lines tested, including 293T, TF-1, and K562 (Fig. 1B and 2E and data not shown). These data suggest that levels of activated hKIT$^{D816V}$ protein are affected posttranslationally in murine cells and, associated with low mutant protein levels, *hKIT$^{D816V}$* alone was unable to efficiently transform murine cells.

The extracellular domains of murine Kit and human KIT share less homology than the intracellular signaling domains and do not bind each others' ligand with equal affinity (21). We considered, first, the possibility that extracellular/transmembrane domains of hKIT$^{D816V}$ might inhibit its transformation potential in murine cells. To test this possibility, we generated two "hybrid KIT" alleles containing the murine *Kit* extracellular and transmembrane domains fused in-frame to the intracellular domain of wild-type human *KIT* (*HyKIT$^{WT}$*) or the D816V mutant (*HyKIT$^{D816V}$*) (Fig. 1A). Proliferation assays demonstrated that replacement of the human extracellular and transmembrane domains of *hKIT$^{D816V}$* with homologous murine sequences (*HyKIT$^{D816V}$*) rescued the transforming ability in murine cells (Fig. 2A). Second, we examined the possibility that the KIT ligand (SCF) might be still required for transformation by *hKIT$^{D816V}$*. However, proliferation assays using

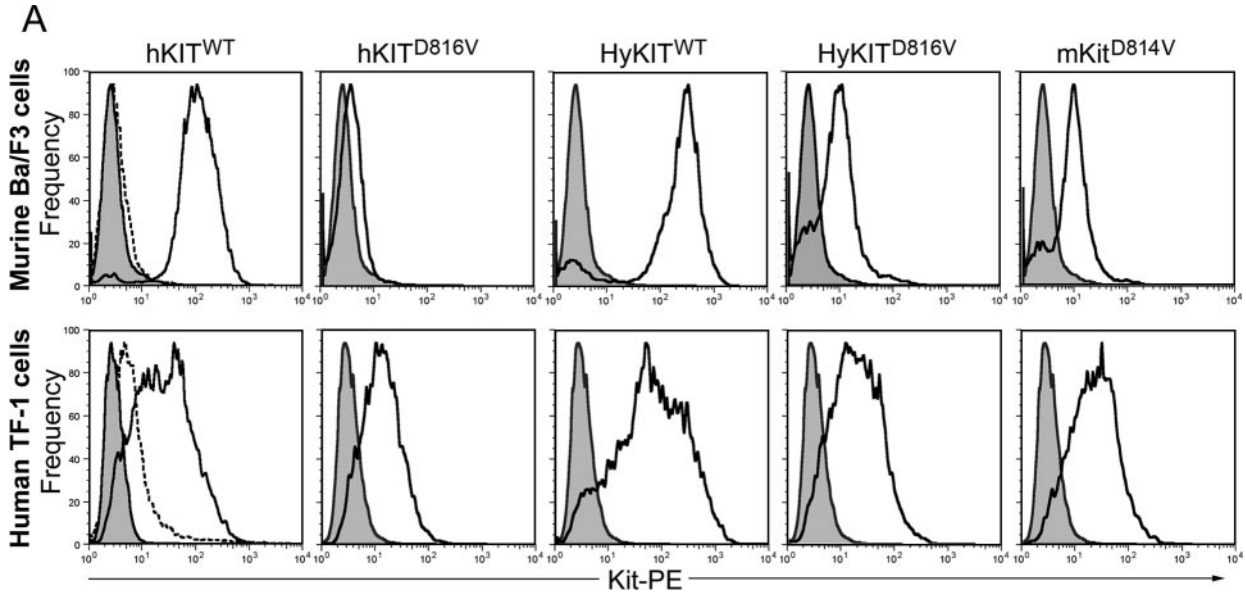


FIG. 4. The transforming potential of different *KIT* alleles is associated with distinct patterns of subcellular KIT receptor localization. (A) Analysis of KIT receptor expression on the cell surface by flow cytometry. Wild-type receptors are expressed at a high level on murine Ba/F3 cells (upper panels) and human TF-1 cells (lower panels). The activated hKIT$^{D816V}$ receptor was not present on the surface of Ba/F3 cells but was present at low levels in TF-1 cells. HyKIT$^{D816V}$ and mKit$^{D814V}$ were present at low/intermediate levels on the surface of both Ba/F3 and TF-1 cells. Shaded curves are isotype control staining. Dashed curves are mocked transduction control staining and represent endogenous KIT expression level. (B) Trafficking of human c-KIT D816V protein is blocked in the ER system in murine cells. Transiently transfected murine NIH 3T3 cells and human A375 cells were costained with anti-c-Kit antibody and anti-calnexin (ER marker) antibody, and all images were taken with a Zeiss LSM510 laser-scanning confocal microscope. Wild-type KIT was localized to the Golgi apparatus and cell surface of both human and murine cells. The hKIT$^{D816V}$ mutant receptor was restricted to the ER of murine cells but was able to traffic to the Golgi apparatus in human cells. HyKIT$^{D816V}$ was present prominently in the Golgi complex and also at the plasma membrane in both murine and human cells. Immunofluorescent staining for mocked controls and vector-only controls was appropriately negative for KIT staining (not shown); the immunofluorescent staining pattern for *HyKIT$^{WT}$*-transfected cells was very similar to *hKIT$^{WT}$*-transfected cells both in murine cells and human cells (not shown); the staining pattern for *mKit$^{D814V}$*-transfected cells was very similar to *HyKIT$^{D816V}$* in both murine cells and human cells (not shown). Arrows, cell plasma membrane staining. (C) Murine NIH 3T3 cells and human A375 cells expressing different *KIT* alleles were costained with anti-c-Kit and anti-GPP130 (Golgi marker) antibodies. Again, hKIT$^{WT}$ was present both at the plasma membrane and the Golgi apparatus. In murine cells, hKIT$^{D816V}$ protein was localized in an ER-specific pattern but colocalized to the Golgi apparatus in human cells. Triangles, Golgi complex staining. (D) Whole-cell lysates prepared from transfected 293T cells were treated with PNGase F and analyzed by immunoblotting following standard protocols. Complete digestion demonstrated that *KIT* alleles used in this study expressed protein products of identical size. CG, complex glycosylated form; HM, high-mannose (immature) form; DG, deglycosylated protein. (E) Whole protein lysates from transfected 293T cells were treated with Endo H. Wild-type KIT receptors are protected from Endo H digestion by mature glycosylation. Mutant KIT$^{D816V}$ (both human and hybrid) and mKit$^{D814V}$ receptors are sensitive to Endo H digestion, indicating an immature, high-mannose glycosylation pattern. These data are consistent with a failure of mutant KIT receptors to traffic normally through the *trans*-Golgi network.

either human KIT ligand or murine Kit ligand demonstrated that both *hKIT$^{D816V}$* and *HyKIT$^{D816V}$* induced cell growth in a cytokine-independent manner (Fig. 3). These results are consistent with previously reported data (28) and confirm that the D816V mutation causes truly ligand-independent activation of the KIT receptor. Taken together, our data suggest that efficient expression and the transforming potential of the KIT$^{D816V}$ protein depends upon species context and that the human extracellular domain of KIT$^{D816V}$ impairs transformation in murine cells.

**Transformation potential of human KIT$^{D816V}$ receptor associated with subcellular localization.** We sought to understand the mechanism by which the extracellular/transmembrane domains of hKIT$^{D816V}$ inhibited its transformation potential in murine cells. Our data suggested that levels of activated hKIT$^{D816V}$ protein were affected posttranslationally by species context and that replacement of the human extracellular and transmembrane domains of *hKIT$^{D816V}$* with homologous murine sequences (i.e., *HyKIT$^{D816V}$*) rescued the impaired expression and transforming ability in murine cells. The half-life of activated mutants of murine Kit receptor is significantly shorter than the half-life of wild-type receptor, yet rapidly degraded murine receptors retain their transforming potential (28), and so we hypothesized that the subcellular localization of mutant KIT receptors might explain our findings. We first used flow cytometry to examine the expression of murine and human KIT proteins at the cell surface (Fig. 4A). The wild-type KIT receptors (both human and hybrid), as expected, were expressed at high levels on the cell surface of murine Ba/F3 cells. The constitutively active mKit$^{D814V}$ and HyKIT$^{D816V}$ receptors were detectable on the cell surface, albeit at reduced levels compared to wild-type receptor (Fig. 4A). In contrast, the hKIT$^{D816V}$ receptor was not significantly expressed on the surface of Ba/F3 cells (Fig. 4A). In human TF-1 cells, this pattern was repeated, except that hKIT$^{D816V}$ was expressed on the cell surface. Furthermore, the cell surface expression pattern of cytokine-independent *HyKIT$^{D816V}$*- and *mKit$^{D814V}$*-transduced Ba/F3 cells did not change after IL-3

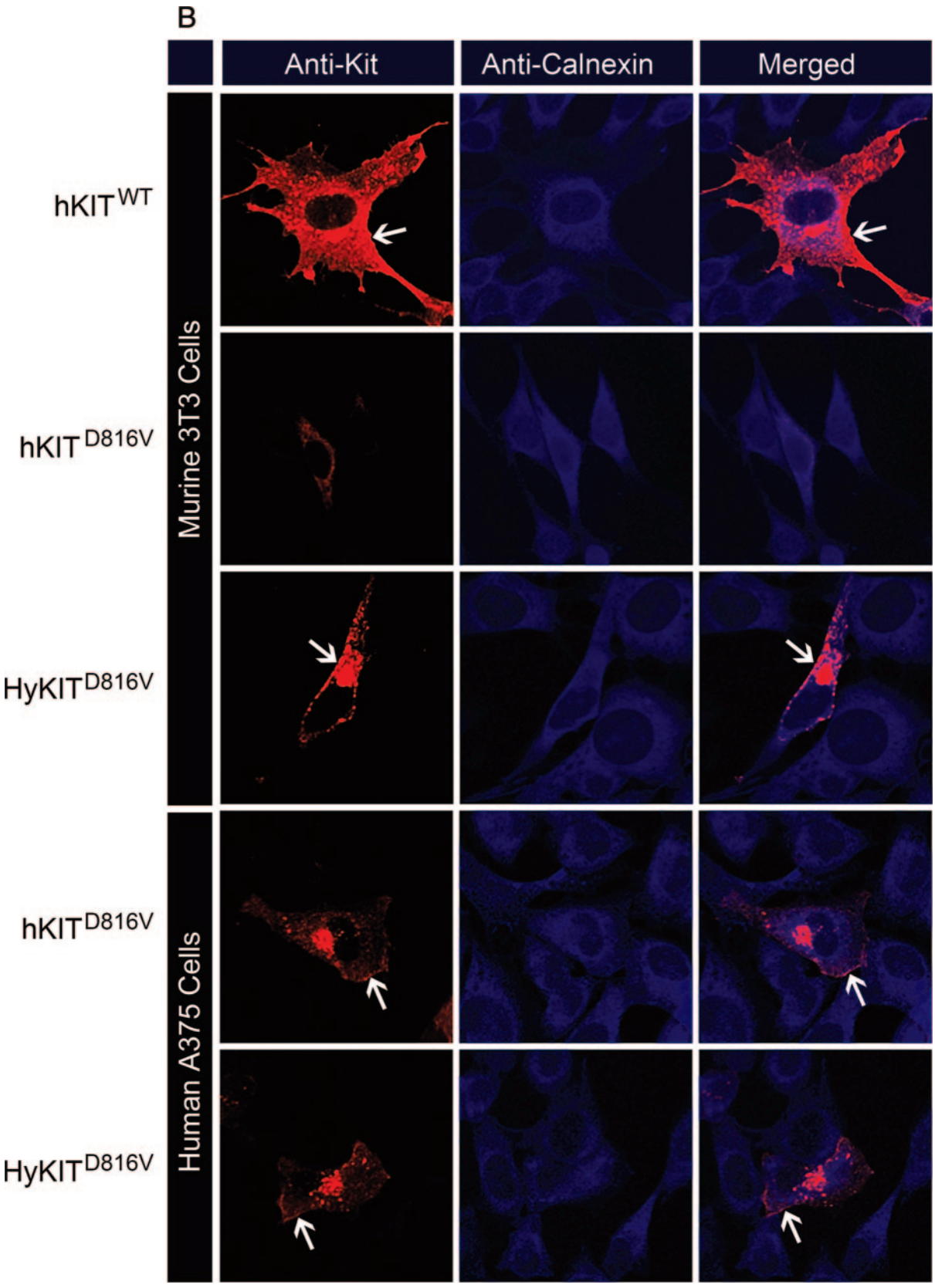


FIG. 4—*Continued.*

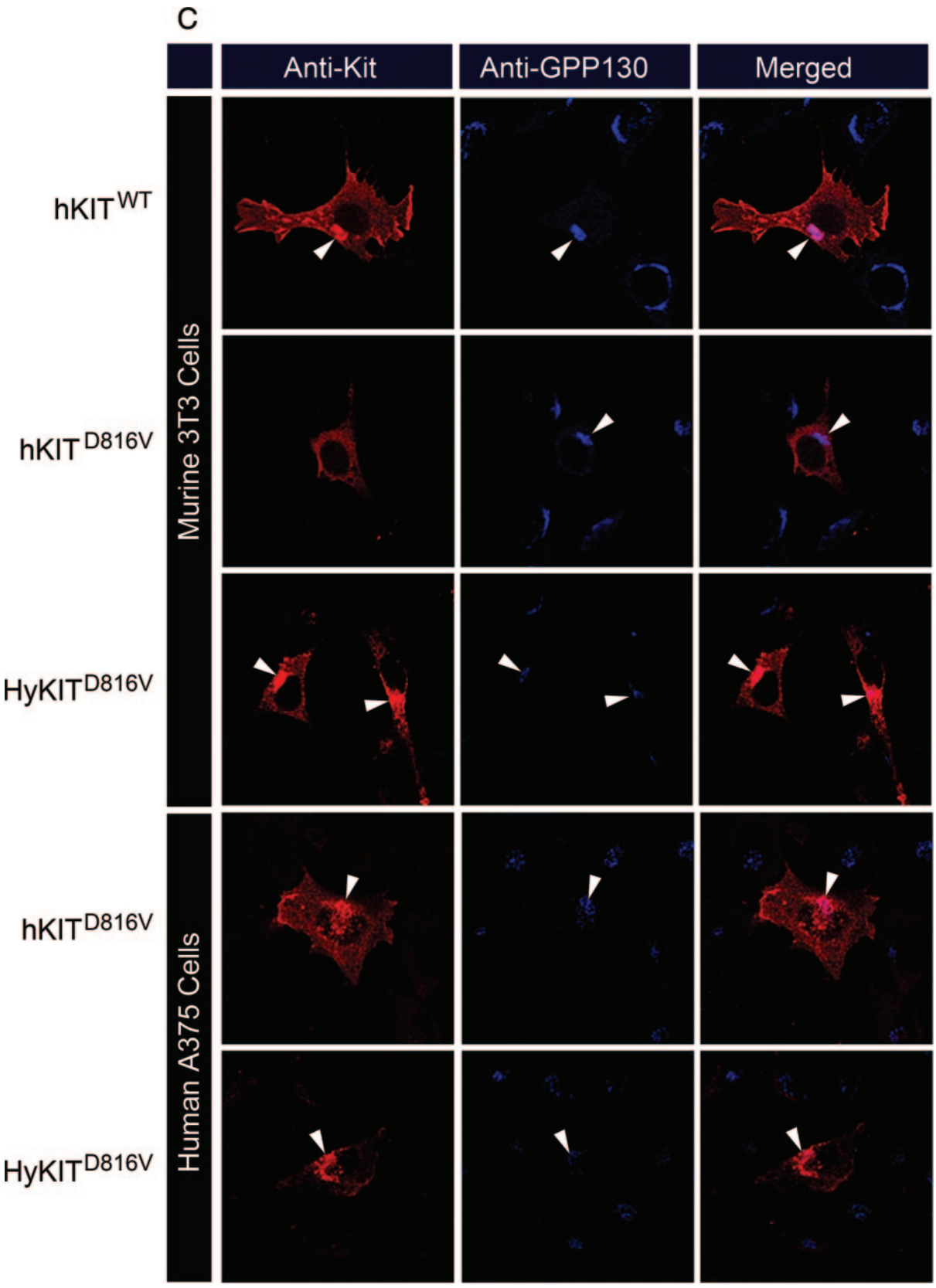


FIG. 4—*Continued.*

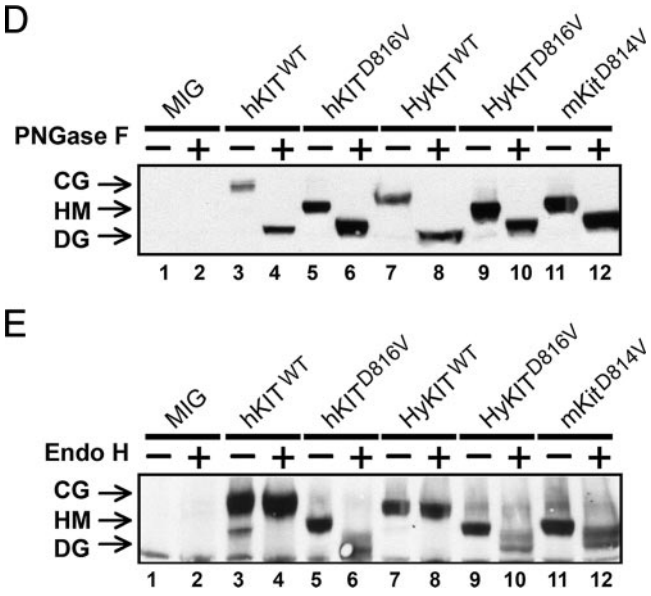


FIG. 4—*Continued.*

starvation, suggesting that those cells lacking KIT surface expression could proliferate with constitutively active KIT signaling from an intracellular compartment (data not shown). We initially hypothesized that mutant KIT might be stabilized in TF-1 cells by the formation of higher-order structures, e.g., heterodimers with endogenous wild-type KIT or erythropoietin (Epo) receptor signaling complexes (39), but we examined a series of cell lines for their ability to express $hKIT^{D816V}$ on their cell surface and found that nonhematopoietic human cells (without endogenous KIT or EpoR expression) allowed surface expression of $hKIT^{D816V}$, while none of the murine cells tested were able to express $hKIT^{D816V}$ on their surface (Table 1). Therefore, the ability of cells to express $hKIT^{D816V}$ at the plasma membrane was not associated with cell type but was consistently associated with the species of origin of the cells in which the mutant KIT was expressed.

We further examined the subcellular localization of KIT receptors directly in murine and human cells using immunofluorescence costaining and confocal microscopy. Using antibodies to costain the KIT receptor and Golgi apparatus or ER, cells expressing wild-type receptors demonstrated a stain pattern consistent with both Golgi and cell surface localization (Fig. 4B and C and data not shown). In sharp contrast, the staining of murine cells expressing $hKIT^{D816V}$ demonstrated an exclusively ER localization pattern. There was a significant difference in the staining pattern in human cells expressing $KIT^{D816V}$, with predominantly Golgi apparatus staining, with a small amount of signal also detected at the cell surface and in punctate cytoplasmic vesicles (Fig. 4B and C). Importantly, $HyKIT^{D816V}$ and $mKIT^{D814V}$ were localized both to Golgi and plasma membrane compartments in both human and murine cells (Fig. 4B and C and data not shown). Consistent with the data obtained from flow cytometry, activated KIT receptors not blocked by the ER (i.e., $hKIT^{D816V}$ in human cells, $HyKIT^{D816V}$, and $mKit^{D814V}$) were present abundantly in the Golgi apparatus but at decreased levels at the plasma membrane. Therefore, replacement of the human extracellular and transmembrane domains of human KIT with the homologous murine sequences allowed trafficking of receptors through the ER to the Golgi apparatus and restored the ability of $KIT^{D816V}$ to transform murine cells.

Progress of glycoproteins through the *cis*- and *trans*-Golgi complex is associated with distinct stages of glycosylation. Different KIT receptor proteins demonstrated similar electrophoretic mobilities following complete digestion of oligosaccharide groups by PNGase F (Fig. 4D). Complex (i.e., mature) oligosaccharide modification can be distinguished from immature high-mannose-type oligosaccharides by digestion with Endo H, which selectively cleaves high-mannose sugars. The wild-type KIT proteins, including $hKIT^{WT}$ and $HyKIT^{WT}$, were resistant to Endo H cleavage, while the activated alleles, including $hKIT^{D816V}$, $HyKIT^{D816V}$, and $mKit^{D814V}$, were sensitive to Endo H digestion (Fig. 4E), indicating that protein maturation of KIT mutants was impaired. Taken together, these data suggest that while wild-type KIT receptors traffic normally through the *trans*-Golgi complex to undergo complex glycosylation, constitutively active KIT proteins are impaired from trafficking through the *trans*-Golgi complex and do not undergo terminal glycosylation. In murine cells expressing $hKIT^{D816V}$, however, the disruption of receptor transport occurred earlier, in the ER, and was more complete, resulting in a total lack of surface expression and a failure to achieve cellular transformation.

**Mutant KIT receptor retained in the ER fails to induce leukemia in mice.** To characterize the ability of murine, human, and hybrid KIT receptors to mediate malignant transformation and disease in vivo, we used ecotropic murine stem cell virus (MSCV) retrovirus to express *KIT* alleles (Fig. 1) in primary murine bone marrow cells and monitored transplanted recipient mice for the development of disease. Consistent with our data demonstrating that $hKIT^{D816V}$ was trapped in the ER and unable to transform murine cells in culture, we found mice transplanted with $hKIT^{D816V}$ did not develop disease (Fig. 5A; Table 2). In sharp contrast, 100% of mice transplanted with $HyKIT^{D816V}$ developed a rapidly fatal MPD with massive expansion of maturing myeloid cells and infiltration of peripheral blood, bone marrow, spleen, liver, and lungs evidenced by leukocytosis, splenomegaly, and increased $GFP^+$ $Mac\text{-}1^+$ cells in peripheral blood, bone marrow, and spleen (Fig. 5A, B, and D, Table 2, and data not shown). All mice transplanted with the $mKIT^{D814V}$ (100%) succumbed to a rapidly fatal leukemia

TABLE 1. c-Kit surface expression in different cell lines[a]

| Allele | Surface expression (% of cells) | | | | |
|---|---|---|---|---|---|
| | Murine | | Human | | |
| | 3T3 | Ba/F3 | 293T | K562 | TF-1 |
| *MIG* | 0.3 | 0.2 | 0.3 | 0.2 | 19.3 |
| $hKIT^{WT}$ | 82.5 | 94.9 | 97.8 | 86.0 | 73.2 |
| $hKIT^{D816V}$ | 3.6 | 5.9 | 79.0 | 49.2 | 50.6 |
| $HyKIT^{WT}$ | 99.4 | 87.1 | 98.6 | 93.5 | 79.6 |
| $HyKIT^{D816V}$ | 30.4 | 35.5 | 66.8 | 49.3 | 55.0 |
| $mKit^{D814V}$ | 49.8 | 36.4 | 87.8 | 57.8 | 61.3 |

[a] A variety of murine and human cell lines were transduced with KIT alleles, and KIT receptor surface expression was assessed by flow cytometry.

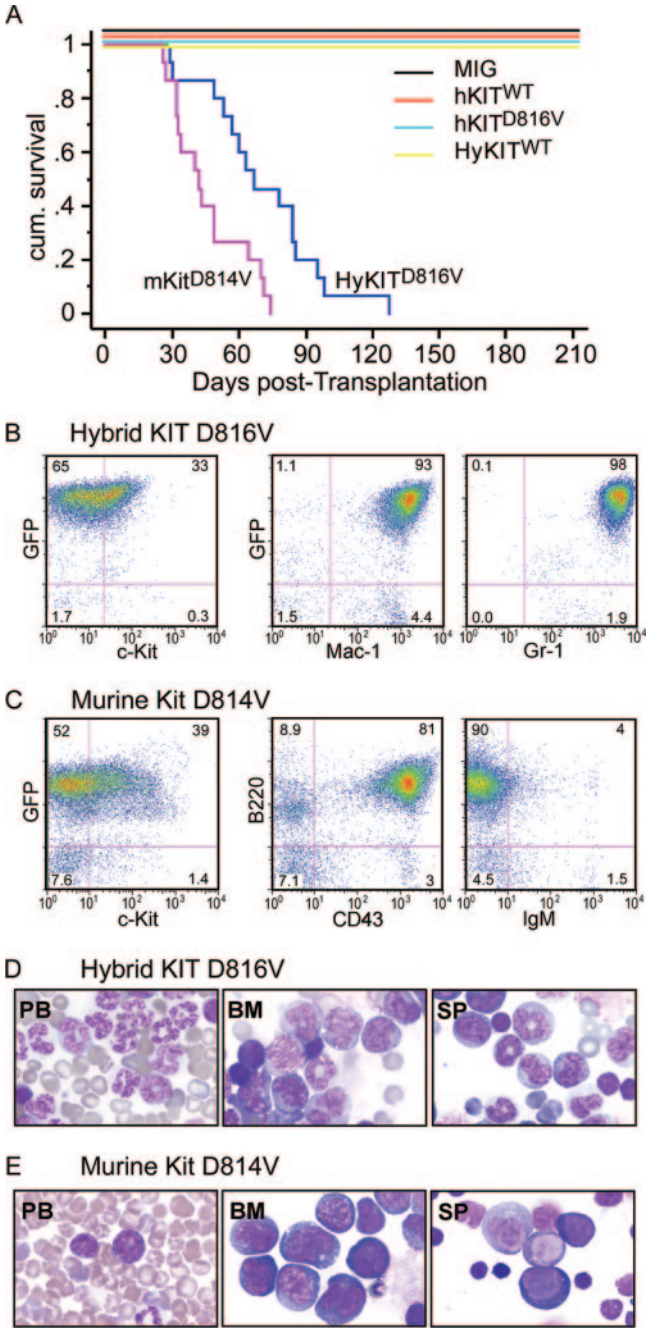


FIG. 5. *KIT* mutants associated with Golgi-localized KIT receptors induce hematopoietic diseases in mice. (A) Kaplan-Meier survival curves of mouse cohorts transplanted with bone marrow transduced with various *KIT* alleles. Three independent transplantations were performed for each construct. Mice transplanted with $HyKIT^{D816V}$-transduced bone marrow mononuclear cells (BMMNC) succumbed to a fatal MPD; mice transplanted with $mKit^{D814V}$-transduced BMMNC developed acute B-lymphocytic leukemia. Mice transplanted with $hKIT^{D816V}$ expressing BMMNC did not succumb to disease after 12 months of observation. (B and C) Immunophenotype analysis of hematopoietic cells from representative sick mice by flow cytometry. (B) Spleen cells from $HyKIT^{D816V}$-induced MPD express predominantly myeloid markers Mac-1 and Gr-1. GFP-positive cells account for 98% of splenocytes, but surface expression of KIT was only detected on 33% of cells. Antibodies used cannot distinguish endogenous Kit from transgenic KIT. (C) Spleen cells from $mkit^{D814V}$-induced disease express pro-B-cell markers B220 and CD43 and are IgM negative. Again, the vast majority of splenocytes (91%) were GFP positive, but only 39% of cells coexpressed GFP and KIT. (D and E) Cell morphology of PB, BM, and SP from representative leukemic mice. (D) Cell morphology of PB, BM, and SP from $HyKIT^{D816V}$-induced MPD mice shows infiltration with myeloid cells. (E) Cell morphology of PB, BM, and SP from $mKit^{D814V}$-induced B-cell leukemia shows infiltration with lymphoid leukemic blasts. No histological abnormality was detected in the $hKIT^{D816V}$-transplanted mice or wild-type control mice (not shown).

as well, characterized by leukocytosis, splenomegaly, and neural system infiltration (Table 2 and data not shown). The leukemia phenotype of mice expressing $mKit^{D814V}$ morphologically and immunophenotypically resembled human pre-B-cell acute lymphocytic leukemia (Fig. 5A, C, and E and Table 2). Notably, although the vast majority of bone marrow and spleen cells from $HyKIT^{D816V}$ and $mKit^{D814V}$ recipient mice were GFP positive (>90%), only about one-third of those $GFP^+$ cells had detectable Kit surface expression when analyzed by flow cytometry (Fig. 5B and C).

**Plasma membrane localization of the KIT receptor is dispensable for leukemia induction.** To better characterize the contribution of localized pools of KIT protein to cellular transformation, we constructed a series of localization domain-tagged KIT mutants by fusing the ICD of KIT in frame to the N-terminal 20-amino-acid palmitoylation domain of GAP-43 (GAP-KIT, targeting to the cell membrane) or to the N-terminal Golgi localization domain of FIG (FIG-KIT, targeting to the Golgi apparatus) (Fig. 6A). All domain-tagged KIT mutants and the ICD alone (ICD-KIT) expressed proteins of expected sizes in human 293T cells (Fig. 6B), and probing with anti-phospho-KIT antibodies demonstrated that KIT truncation and heterologous domain fusion by itself did not induce receptor auto-activation. However, KIT proteins with the D816V mutation were constitutively phosphorylated (Fig. 6B). We confirmed successful targeting of localization domain-tagged KIT proteins to specific cellular compartments by confocal microscopy. As anticipated, FIG-$KIT^{WT}$ was localized to the Golgi apparatus, GAP-$KIT^{WT}$ was localized to the plasma membrane, and ICD-$KIT^{WT}$, lacking a signal peptide and transmembrane domain, was found diffusely in the cytoplasm (Fig. 6C). Constitutive activation did not affect the Golgi localization pattern of FIG-KIT or the cytoplasmic localization of ICD-KIT. However, GAP-$KIT^{D816V}$, unlike its wild-type counterpart, was found localized to the Golgi apparatus (Fig. 6C). Therefore, trafficking of activated GAP-$KIT^{D816V}$ to the plasma membrane was abrogated independently of the extracellular domain by an unknown mechanism.

We sought to determine the functional significance of KIT proteins localized to specific cellular compartments by expressing localization domain-tagged KIT proteins in Ba/F3 cells and in the bone marrow of mice by using retroviral transduction/bone marrow transplantation. Localization domain-tagged KIT proteins containing the wild-type ICD failed to transform Ba/F3 cells to factor independence following IL-3 withdrawal (data not shown). In contrast, Golgi-localized FIG-$KIT^{D816V}$ transformed Ba/F3 cells to IL-3 independence with similar growth kinetics to $HyKIT^{D816V}$. GAP-$KIT^{D816V}$ also allowed factor-independent growth, albeit at a slower rate (Fig. 6D).

TABLE 2. Clinicopathological features of diseases induced by c-Kit mutations

| Kit mutant | *n* | Median survival (days) | PB WBC[a] ($10^3/\mu l$) | Spleen wt (mg) | Infiltration | | Paralysis |
|---|---|---|---|---|---|---|---|
| | | | | | Liver[b] | Lung[b] | |
| $hKIT^{D816V}$ | 15 | NED[c] | 7.9 ± 1.9 | 80 ± 10 | − | − | − |
| $HyKIT^{D816V}$ | 15 | 68 ± 22 | 386 ± 235 | 1,070 ± 185 | ++++ | +++ | 2/15 |
| $mKit^{D814V}$ | 15 | 46 ± 17 | 40 ± 80 | 445 ± 231 | − | ++ | 9/15 |
| ICD-$KIT^{D816V}$ | 10 | 43 ± 23 | 217 ± 147 | 600 ± 53 | +++ | ++ | − |

[a] PB WBC, peripheral blood white blood count.
[b] Liver and lung infiltration levels were assessed by microscopic examination of formalin-fixed, hematoxylin and eosin-stained tissue sections.
[c] NED, no evidence of disease.

Surprisingly, cytosol-localized ICD-$KIT^{D816V}$ also transformed Ba/F3 cells to factor independence (Fig. 6D). We performed retroviral transduction/bone marrow transplantation using ICD-KIT and ICD-$KIT^{D816V}$. Mice transplanted with ICD-$KIT^{D816V}$ rapidly and uniformly succumbed to fatal MPD with a median survival similar to that for $mKit^{D814V}$ disease mice (Fig. 6E and F and Table 2), while ICD-$KIT^{WT}$ mice survived normally, demonstrating in vivo KIT-mediated transformation is independent of the secretory pathway entirely. These data demonstrate that Golgi localization is sufficient and plasma membrane localization is dispensable for $KIT^{D816V}$-driven transformation.

**Intracellular trafficking modulates downstream signaling by the $KIT^{D816V}$ receptor.** Transformation of cells by KIT activation is ultimately mediated by downstream signaling pathways (22), and we sought to characterize the signaling pathways activated by transforming versus nontransforming *KIT* alleles. We used Western blotting with phospho-specific antibodies to examine the activation status of downstream signaling pathways in Ba/F3 cells expressing the transforming *HyKIT*$^{D816V}$ and the nontransforming *hKIT*$^{D816V}$. We found Akt, Stat3, and Stat5 signaling was activated by $HyKIT^{D816V}$, but these pathways were activated to a lesser extent, or not at all, by $hKIT^{D816V}$ (Fig. 7A). In contrast, we observed equivalent or perhaps even increased levels of MAPK signaling, as measured by phospho-ERK antibody, in cells expressing the ER-localized $hKIT^{D816V}$ (Fig. 7A). Using a high-affinity monoclonal antibody directed toward the phosphorylated consensus binding sequence of the PI3K p85 subunit, we observed dramatic increases in the abundance of proteins expressing this epitope in all cells expressing activated *KIT* alleles, including *hKIT*$^{D816V}$ (Fig. 7A). Therefore, expression of the ER-localized $hKIT^{D816V}$ was sufficient to activate certain downstream signaling pathways (e.g., MAPK-ERK, p85 binding epitope), but activation of other pathways (e.g., Stat3, Stat5, and Akt) required trafficking past the ER.

We sought to determine the relative contributions of the Golgi apparatus and cell surface pools of mutant KIT receptor to malignant transformation. We treated 3T3 cells expressing the transformation-competent membrane/Golgi-localized *HyKIT*$^{D816V}$ or cytosol-localized *ICD-KIT*$^{D816V}$ with monensin or brefeldin A (BFA), compounds that disrupt Golgi structure via different mechanisms, and assessed the impact of these disruptions on the activation of downstream signaling pathways. Treatment with BFA, which causes fusion and retrograde transport of resident proteins from the Golgi complex to the ER (23), completely eliminated downstream Akt, MAPK, and Stat3 signaling in $HyKIT^{D816V}$-expressing cells but not ICD-$KIT^{D816V}$-expressing cells (Fig. 7B and C). In contrast, monensin treatment, which preferentially affects the *trans*-Golgi network and disrupts secretory vesicle transport to the plasma membrane (27), had little effect on Akt, MAPK, and Stat3 signaling by both $HyKIT^{D816V}$ and ICD-$KIT^{D816V}$ (Fig. 7D and E). Therefore, BFA treatment mimicked the phenomenon we noted with $hKIT^{D816V}$ in murine cells, i.e., oncogenic signaling was disrupted by mislocalization of mutant KIT to the ER. In contrast, disruption of vesicular transport from the *trans*-Golgi network to the cell surface by monensin did not significantly affect signaling by mutant KIT. Taken together, these data demonstrate that plasma membrane localization is dispensable for intracellular signaling activation by mutant KIT receptor.

## DISCUSSION

Recent data have demonstrated that phosphorylation of the FLT3 ITD results in aberrant intracellular receptor trafficking (34). Here, we present the first data demonstrating the functional consequences of aberrant RTK localization. Expression of *hKIT*$^{D816V}$ rapidly transformed human hematopoietic cells to factor independence but was not sufficient to transform murine Ba/F3 cells in short-term assays. Murine cells, but not human cells, localized the $hKIT^{D816V}$ protein exclusively to the ER, while $HyKIT^{D816V}$ and $mKIT^{D814V}$ were transported through the Golgi apparatus. In contrast to wild-type KIT receptor, activated $mKit^{D814V}$ and $HyKIT^{D816V}$ receptors were expressed at low levels at the plasma membrane and were predominantly immature glycosylated forms consistent with a partial block of transport in the Golgi complex. We confirmed that wild-type KIT receptor is a surface glycoprotein resistant to Endo H cleavage, consistent with mature glycosylation obtained through a complex series of modifications that occur in the *trans*-Golgi system. In contrast, the human, murine, and hybrid KIT mutant receptors were significantly sensitive to Endo H digestion, demonstrating a failure to achieve a mature glycosylation pattern consistent with the model that constitutively activated KIT receptors do not traffic normally through the *trans*-Golgi network. The failure of constitutively active RTKs to traffic through the Golgi apparatus is not complete. We observed two biochemically distinct pools of receptor: immature (i.e., high-mannose) receptor and a smaller pool of completely glycosylated receptor that coincides with detection at the plasma membrane. Data from flow cytometry, immunofluorescence, and endoglycosidase experiments were consis-

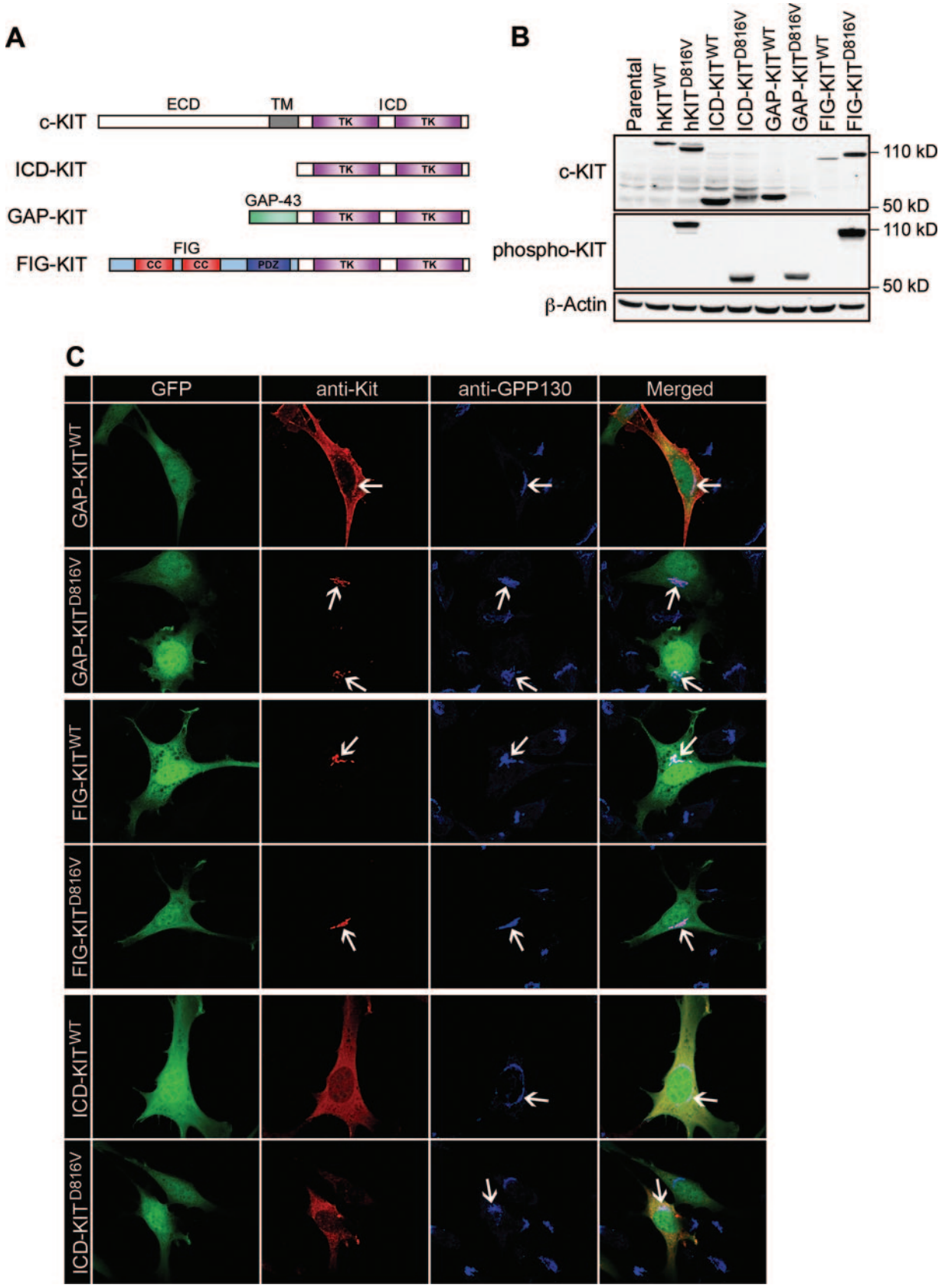

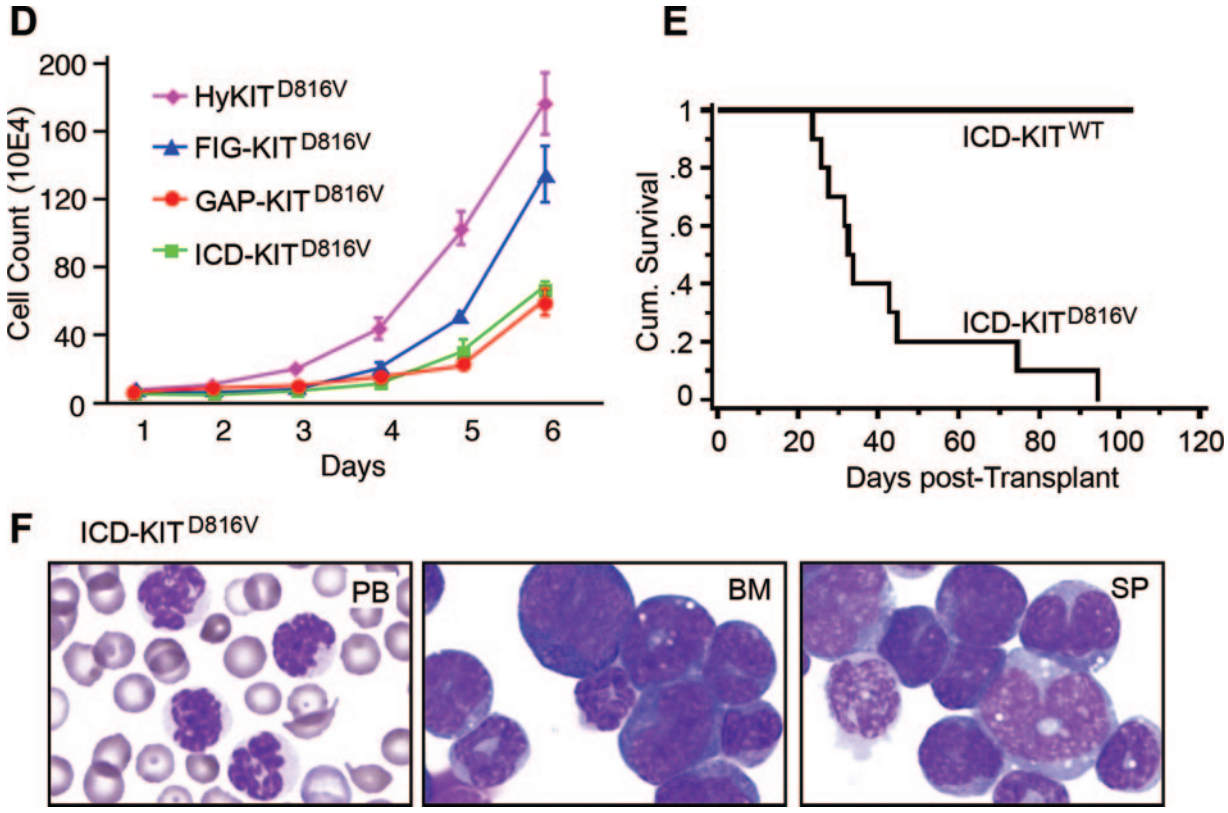


FIG. 6. Plasma membrane localization is dispensable for mutant KIT-induced neoplasia. (A) Schematic diagram of domain-tagged *KIT* allele targeting constructs. The KIT receptor consists of an extracellular domain (ECD), a transmembrane domain (TM), and an intracellular domain (ICD) which has two tyrosine kinase domains (TK). *ICD-KIT* only expresses the truncated intracellular portion of the KIT receptor; the GAP-KIT fusion protein fuses the first 20 amino acids of GAP-43 in frame to the KIT ICD; the FIG-KIT fusion protein fuses the majority (90%) of FIG in frame to the KIT ICD. CC, coiled-coil domain; PDZ, PDZ domain. (B) Western blot of total cell lysates from 293T cells expressing each domain-tagged *KIT* allele targeting construct. Full-length $hKIT^{WT}$ and $hKIT^{D816V}$ were used as positive control. Molecular weights of mutant domain-tagged *KIT* alleles were bigger than wild-type counterparts, probably due to posttranslational modification (i.e., phosphorylation), which also altered the binding capacity to anti-total Kit antibody. All *D816V* alleles are highly phosphorylated. (C) Protein localization analysis by immunofluorescent staining and confocal microscopy. NIH 3T3 cell transfection and immunofluorescent staining were performed as described for Fig. 4, and all images were taken with a Zeiss LSM510 laser scanning confocal microscopy. Arrows indicate Golgi colocalization of KIT protein. (D) Transformation potential of each targeting *KIT* allele. Murine Ba/F3 cells were transduced and sorted based on the same GFP expression level, IL-3 was removed from growth medium, and viable cells were counted daily. Parental Ba/F3 cells, Ba/F3 cells transduced with vector alone, and wild-type alleles could not grow in the absence of IL-3 (data not shown). (E) The intracellular portion alone of mutant KIT receptor is able to induce MPD in mice. Phenotype was confirmed by histopathology, flow cytometry (data not shown), and cell morphology. (F) Cell morphology of PB, BM, and SP from an $ICD\text{-}KIT^{D816V}$-induced MPD mouse indicates predominantly mature myeloid cells.

tent and supported a model of KIT receptor trafficking dependent upon phosphorylation as well as species context (Fig. 2, 4, and 7). We used BFA and monensin to disrupt Golgi processing at distinct points to characterize the functional significance of these different KIT forms. Complete Golgi disruption with BFA abolished downstream Akt, MAPK, and Stat3 signaling by chemically localizing the receptor in the ER, effectively mimicking the result we observed with ER-localized $hKIT^{D816V}$. In contrast, monensin disruption of the *trans*-Golgi network and vesicular transport to the plasma membrane had minimal effect on the activation of leukemia-associated downstream signaling (Fig. 7). Furthermore, the D816V mutation artificially targeted to the Golgi apparatus ($FIG\text{-}KIT^{D816V}$) and even cytosolic form ($ICD\text{-}KIT^{D816V}$) were biologically active in vitro and in vivo. These results suggest that the Golgi-localized immature KIT form is necessary and sufficient to induce leukemogenic signals. In contrast $hKIT^{D816V}$, trapped in the ER, was unable to cause disease in mice. However, despite poor surface expression, $mKit^{D814V}$ and $HyKIT^{D816V}$ uniformly induced fatal leukemias. The *HyKIT* oncogene that we describe here will be useful for studying the mechanisms by which *KIT* mutations contribute to the transformation of primary murine cells, e.g., in core binding factor leukemias.

The extracellular/transmembrane domains of KIT were critical for subcellular localization and leukemogenesis, but it was unclear why $mKit^{D814V}$ and $HyKIT^{D816V}$ with identical extracellular and transmembrane domains caused distinct phenotypes (B-lymphoid versus MPD) when expressed in mice (Fig. 6). To assess differences between the murine and human intracellular domains that might be functionally relevant, we used a neural network program to predict sites of tyrosine phosphorylation (6). Ten conserved tyrosines were identified in the *mKit* cytoplasmic tail that were predicted phosphorylation targets on the basis of surrounding consensus sequences.

A single amino acid substitution (D747G) in *hKIT* significantly disrupted the consensus sequence for phosphorylation of tyrosine 749 (murine score, 0.713; human score, 0.199). As a result, *hKIT* contains one less consensus tyrosine phosphorylation site than *mKit* (9 versus 10). Therefore, the different leukemia phenotypes induced by $mKit^{D814V}$ and $HyKIT^{D816V}$ may be due to differential binding of an unidentified SH2 domain-containing signaling intermediate at tyrosine 749.

**The Golgi apparatus is an important source of leukemogenic signals.** Because ligand-mediated activation of cytokine receptors occurs at the cell surface, it is generally assumed that activation of canonical signaling pathways by mutant receptors requires plasma membrane localization. However, increasing evidence has suggested that cell surface binding of the receptor may be dispensable for transformation. The simian sarcoma virus gene product v-Sis induces autocrine activation of platelet-derived growth factor receptor (4, 14, 16, 40). The FIG-ROS fusion protein is expressed as a result of a chromosome 6 microdeletion in a neuroblastoma cell line and involves activation of the c-Ros RTK by receptor localization to the Golgi apparatus, and this Golgi localization is sufficient and required for cellular transformation mediated by FIG-ROS (8). Recently, noncanonical activation of the Ras/MAPK pathway has been found to occur at the endosome and the Golgi apparatus, and that compartmentalized Ras signaling may modulate distinct functional outcomes (30). Here, we showed that mutant KIT proteins were predominantly localized to the Golgi apparatus and present only at low abundance on the cell surface. We further targeted KIT expression specifically to the Golgi compartment and found that FIG-$KIT^{D816V}$ could transform Ba/F3 cells to cytokine independence (Fig. 6D). We also performed retroviral transduction/bone marrow transplantation using other domain-tagged KIT constructs (*GAP-KIT* and *FIG-KIT*). Preliminary data showed that both Golgi-localized GAP-$KIT^{D816V}$ and FIG-$KIT^{D816V}$ could cause diseases in mice (unpublished data). Both in vitro and in vivo data clearly support that Golgi localization is sufficient for $KIT^{D816V}$-driven transformation. We also used monensin and brefeldin A to inhibit protein transport from the Golgi apparatus and ER, respectively and, consistent with our transformation data, found that Golgi localization, not plasma membrane localization, was required to activate downstream signaling pathways. We cannot exclude the possibility that important signals may also be contributed by post-Golgi transport vesicles, but the amount of KIT protein detected in these vesicles by immunofluorescence was small. Taken together, these data demonstrate that intracellular compartments, such as the Golgi apparatus, are important contexts for oncogenic signaling events previously thought to be exclusive to the plasma membrane. The mechanisms by which oncogenic RTKs activate downstream signaling pathways such as Ras/MAPK and PI3K/Akt, independent of the plasma membrane, remain to be determined.

Our results may be relevant to the treatment of human cancers driven by mutant RTKs. Our data predict that RTK-driven cancers may acquire resistance to extracellular domain-targeted antibody therapies, such as Herceptin, by mechanisms to downregulate or eliminate cell surface expression. Also, our results suggest that the ER misfolded protein checkpoint may represent a novel therapeutic target for patients expressing activated RTK mutations. A subtle shift in KIT receptor trafficking was sufficient to convert the $hKIT^{D816V}$ gene product from cancer initiator to an apparently harmless misfolded protein. Strong blockade of the secretory apparatus would likely be highly toxic, but a therapeutic window might be identi-

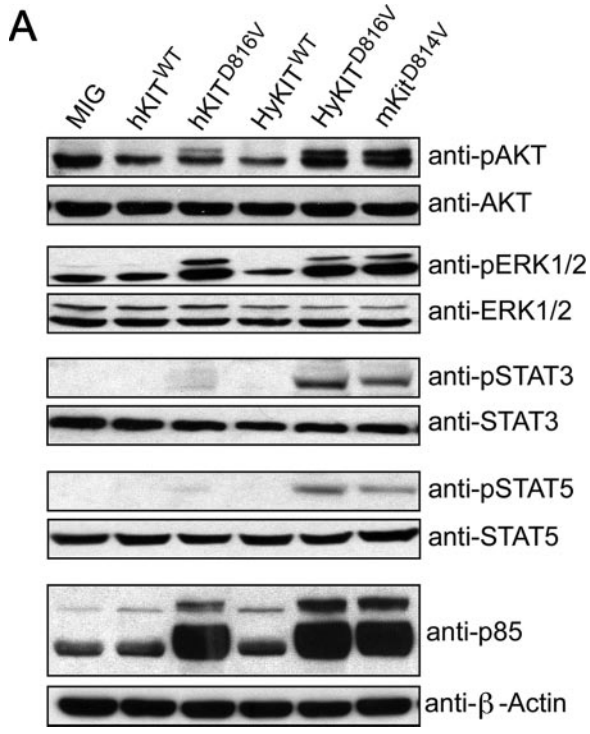


FIG. 7. Subcellular localization of mutant KIT protein affects downstream signal transduction. (A) Downstream signal transduction pathways activated by various *KIT* alleles. Ba/F3 cells expressing various *KIT* alleles or vector alone were starved of IL-3 overnight, and total cell lysates were analyzed by SDS-PAGE and blotted with phospho-specific antibodies and total antibodies. ER-localized $hKIT^{D816V}$ strongly activates ERK and the PI3K consensus binding motif but does not strongly activate Akt, Stat3, and Stat5. Golgi/plasma membrane-localized $HyKIT^{D816V}$ and $mKit^{D814V}$ activate Akt, Stat3, and Stat5 pathways. (B and C) Dissection of signaling pathways activated by mutant KIT after inhibiting protein transport by BFA. NIH 3T3 cells transduced with retroviral supernatant were treated with 5 μg/ml BFA for 20 h, a single-cell suspension was prepared for flow cytometry analysis, and total cell lysates were prepared for signaling analysis following a standard protocol described previously. (B) Flow cytometry analysis of KIT surface expression in NIH 3T3 cells with or without BFA treatment. BFA completely blocked KIT receptor transport to the cell surface. Gray line, isotype control; dashed line, with BFA treatment; solid line, no BFA. (C) Downstream Akt, Erk, and Stat3 signaling was completely abrogated in $HyKIT^{D816V}$-expressing cells but not in ICD-$KIT^{D816V}$ cells by Golgi disruption and retrograde transport to the ER induced by BFA. (D and E) Mosensin had a minimal effect on downstream signaling activation mediated by KIT mutants. NIH 3T3 cells transduced with retroviral supernatant were treated with 3 μM monensin for 48 h, a single-cell suspension was prepared for flow cytometry analysis, and total cell lysates were prepared for signaling analysis following a standard protocol described previously. (D) Flow cytometry analysis of KIT surface expression in NIH 3T3 cells with or without monensin treatment. Monensin significantly reduced KIT receptor expression by 96% at the cell surface. Gray line, isotype control; long dashed line, with monensin treatment; solid line, no monensin. (E) Monensin had little effect on downstream Akt, ERK, and Stat3 signaling activated by mutant Kit receptors.

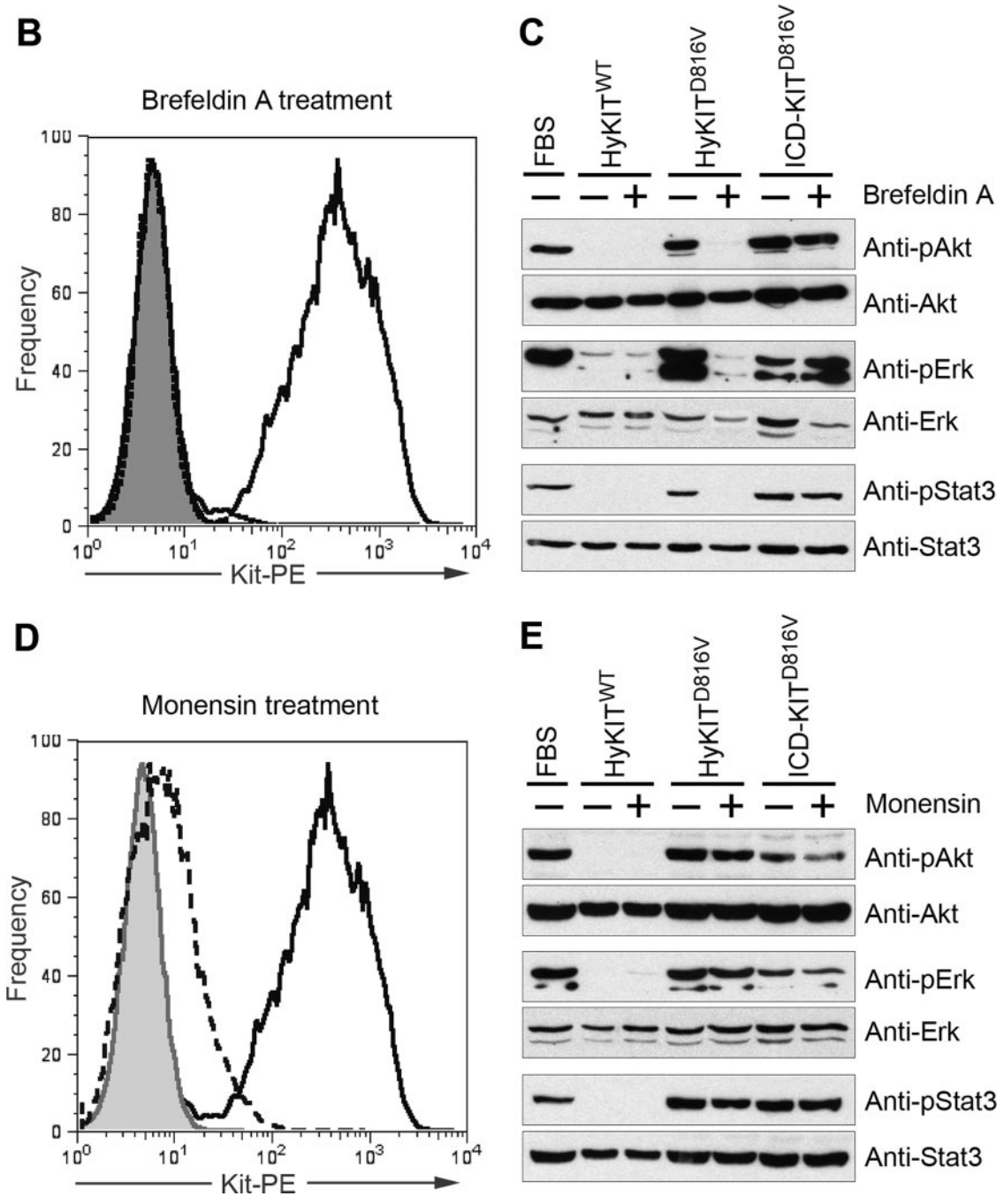


FIG. 7—*Continued.*

fied; a partial chemical block might interfere specifically with the processing and localization of pathogenic oncoproteins. Understanding the molecular mechanism by which mutant *KIT* alleles activate disease-causing downstream signaling pathways will allow us to identify and test novel therapeutic strategies.


## ACKNOWLEDGMENTS

We thank Stuart Kornfeld, Linda Pike, Thomas Jahn, and Paddy Ross for valuable discussions and Timothy Ley, Timothy Graubert, Katherine Weilbaecher, Daniel Link, and Julie O'Neal for critical reading of the manuscript. Leonie Ashman and Masao Mizuki provided valuable reagents. We are grateful to Richard Steet for technical assistance with immunofluorescence staining and Bill Eades for assistance with flow cytometry.

This work was supported by NIH grant P01 CA 101937-01 (M.H.T.).


## REFERENCES


1. **Beghini, A., L. Larizza, R. Cairoli, and E. Morra.** 1998. c-kit activating mutations and mast cell proliferation in human leukemia. Blood **92:**701–702.
2. **Beghini, A., P. Peterlongo, C. B. Ripamonti, L. Larizza, R. Cairoli, E. Morra, and C. Mecucci.** 2000. c-kit mutations in core binding factor leukemias. Blood **95:**726–727.

3. **Beghini, A., C. B. Ripamonti, R. Cairoli, G. Cazzaniga, P. Colapietro, F. Elice, G. Nadali, G. Grillo, O. A. Haas, A. Biondi, E. Morra, and L. Larizza.** 2004. KIT activating mutations: incidence in adult and pediatric acute myeloid leukemia, and identification of an internal tandem duplication. Haematologica **89:**920–925.
4. **Bejcek, B. E., D. Y. Li, and T. F. Deuel.** 1989. Transformation by v-sis occurs by an internal autoactivation mechanism. Science **245:**1496–1499.
5. **Besmer, P., J. E. Murphy, P. C. George, F. H. Qiu, P. J. Bergold, L. Lederman, H. W. Snyder, Jr., D. Brodeur, E. E. Zuckerman, and W. D. Hardy.** 1986. A new acute transforming feline retrovirus and relationship of its oncogene v-kit with the protein kinase gene family. Nature **320:**415–421.
6. **Blom, N., S. Gammeltoft, and S. Brunak.** 1999. Sequence and structure-based prediction of eukaryotic protein phosphorylation sites. J. Mol. Biol. **294:**1351–1362.
7. **Broudy, V. C.** 1997. Stem cell factor and hematopoiesis. Blood **90:**1345–1364.
8. **Charest, A., V. Kheifets, J. Park, K. Lane, K. McMahon, C. L. Nutt, and D. Housman.** 2003. Oncogenic targeting of an activated tyrosine kinase to the Golgi apparatus in a glioblastoma. Proc. Natl. Acad. Sci. USA **100:**916–921.
9. **Corbin, A. S., I. J. Griswold, P. La Rosee, K. W. Yee, M. C. Heinrich, C. L. Reimer, B. J. Druker, and M. W. Deininger.** 2004. Sensitivity of oncogenic KIT mutants to the kinase inhibitors MLN518 and PD180970. Blood **104:** 3754–3757.
10. **Ferrao, P., T. J. Gonda, and L. K. Ashman.** 1997. Expression of constitutively activated human c-Kit in Myb transformed early myeloid cells leads to factor independence, histiocytic differentiation, and tumorigenicity. Blood **90:**4539–4552.
11. **Furitsu, T., T. Tsujimura, T. Tono, H. Ikeda, H. Kitayama, U. Koshimizu, H. Sugahara, J. H. Butterfield, L. K. Ashman, Y. Kanayama, et al.** 1993. Identification of mutations in the coding sequence of the proto-oncogene c-kit in a human mast cell leukemia cell line causing ligand-independent activation of c-kit product. J. Clin. Investig. **92:**1736–1744.
12. **Geissler, E. N., M. A. Ryan, and D. E. Housman.** 1988. The dominant-white spotting (W) locus of the mouse encodes the c-kit proto-oncogene. Cell **55:**185–192.
13. **Grisolano, J. L., J. O'Neal, J. Cain, and M. H. Tomasson.** 2003. An activated receptor tyrosine kinase, TEL/PDGFβR, cooperates with AML1/ETO to induce acute myeloid leukemia in mice. Proc. Natl. Acad. Sci. USA **100:** 9506–9511.
14. **Hart, K. C., Y. F. Xu, A. N. Meyer, B. A. Lee, and D. J. Donoghue.** 1994. The v-sis oncoprotein loses transforming activity when targeted to the early Golgi complex. J. Cell Biol. **127:**1843–1857.
15. **Kanakura, Y., T. Furitsu, T. Tsujimura, J. H. Butterfield, L. K. Ashman, H. Ikeda, H. Kitayama, Y. Kanayama, Y. Matsuzawa, and Y. Kitamura.** 1994. Activating mutations of the c-kit proto-oncogene in a human mast cell leukemia cell line. Leukemia **8**(Suppl. 1)**:**S18–S22.
16. **Keating, M. T., and L. T. Williams.** 1988. Autocrine stimulation of intracellular PDGF receptors in v-sis-transformed cells. Science **239:**914–916.
17. **Kitayama, H., Y. Kanakura, T. Furitsu, T. Tsujimura, K. Oritani, H. Ikeda, H. Sugahara, H. Mitsui, Y. Kanayama, Y. Kitamura, et al.** 1995. Constitutively activating mutations of c-kit receptor tyrosine kinase confer factor-independent growth and tumorigenicity of factor-dependent hematopoietic cell lines. Blood **85:**790–798.
18. **Kitayama, H., T. Tsujimura, I. Matsumura, K. Oritani, H. Ikeda, J. Ishikawa, M. Okabe, M. Suzuki, K. Yamamura, Y. Matsuzawa, Y. Kitamura, and Y. Kanakura.** 1996. Neoplastic transformation of normal hematopoietic cells by constitutively activating mutations of c-kit receptor tyrosine kinase. Blood **88:**995–1004.
19. **Kosmider, O., N. Denis, C. Lacout, W. Vainchenker, P. Dubreuil, and F. Moreau-Gachelin.** 2005. Kit-activating mutations cooperate with Spi-1/PU.1 overexpression to promote tumorigenic progression during erythroleukemia in mice. Cancer Cell **8:**467–478.
20. **Lev, S., J. Blechman, S. Nishikawa, D. Givol, and Y. Yarden.** 1993. Interspecies molecular chimeras of kit help define the binding site of the stem cell factor. Mol. Cell. Biol. **13:**2224–2234.
21. **Lev, S., Y. Yarden, and D. Givol.** 1992. Dimerization and activation of the kit receptor by monovalent and bivalent binding of the stem cell factor. J. Biol. Chem. **267:**15970–15977.
22. **Linnekin, D.** 1999. Early signaling pathways activated by c-Kit in hematopoietic cells. Int. J. Biochem. Cell Biol. **31:**1053–1074.
23. **Lippincott-Schwartz, J., L. C. Yuan, J. S. Bonifacino, and R. D. Klausner.** 1989. Rapid redistribution of Golgi proteins into the ER in cells treated with brefeldin A: evidence for membrane cycling from Golgi to ER. Cell **56:**801–813.
24. **Longley, B. J., L. Tyrrell, S. Z. Lu, Y. S. Ma, K. Langley, T. G. Ding, T. Duffy, P. Jacobs, L. H. Tang, and I. Modlin.** 1996. Somatic c-KIT activating mutation in urticaria pigmentosa and aggressive mastocytosis: establishment of clonality in a human mast cell neoplasm. Nat. Genet. **12:**312–314.
25. **Luo, H., Q. Li, J. O'Neal, F. Kreisel, M. M. Le Beau, and M. H. Tomasson.** 2005. c-Myc rapidly induces acute myeloid leukemia in mice without evidence of lymphoma-associated antiapoptotic mutations. Blood **106:**2452–2461.
26. **Majumder, S., K. Brown, F. H. Qiu, and P. Besmer.** 1988. c-kit protein, a transmembrane kinase: identification in tissues and characterization. Mol. Cell. Biol. **8:**4896–4903.
27. **Mollenhauer, H. H., D. J. Morre, and L. D. Rowe.** 1990. Alteration of intracellular traffic by monensin; mechanism, specificity and relationship to toxicity. Biochim. Biophys. Acta **1031:**225–246.
28. **Moriyama, Y., T. Tsujimura, K. Hashimoto, M. Morimoto, H. Kitayama, Matsuzawa, Y. Kitamura, and Y. Kanakura.** 1996. Role of aspartic acid 814 in the function and expression of c-kit receptor tyrosine kinase. J. Biol. Chem. **271:**3347–3350.
29. **Nakai, Y., N. Nonomura, D. Oka, M. Shiba, Y. Arai, M. Nakayama, H. Inoue, K. Nishimura, K. Aozasa, Y. Mizutani, T. Miki, and A. Okuyama.** 2005. KIT (c-kit oncogene product) pathway is constitutively activated in human testicular germ cell tumors. Biochem. Biophys. Res. Commun. **337:**289–296.
30. **Philips, M. R.** 2005. Compartmentalized signalling of Ras. Biochem. Soc. Trans. **33:**657–661.
31. **Qiu, F. H., P. Ray, K. Brown, P. E. Barker, S. Jhanwar, F. H. Ruddle, and P. Besmer.** 1988. Primary structure of c-kit: relationship with the CSF-1/PDGF receptor kinase family—oncogenic activation of v-kit involves deletion of extracellular domain and C terminus. EMBO J. **7:**1003–1011.
32. **Reilly, J. T.** 2002. Class III receptor tyrosine kinases: role in leukaemogenesis. Br. J. Haematol. **116:**744–757.
33. **Rubin, B. P., S. Singer, C. Tsao, A. Duensing, M. L. Lux, R. Ruiz, M. K. Hibbard, C. J. Chen, S. Xiao, D. A. Tuveson, G. D. Demetri, C. D. Fletcher, and J. A. Fletcher.** 2001. KIT activation is a ubiquitous feature of gastrointestinal stromal tumors. Cancer Res. **61:**8118–8121.
34. **Schmidt-Arras, D. E., A. Bohmer, B. Markova, C. Choudhary, H. Serve, and F. D. Bohmer.** 2005. Tyrosine phosphorylation regulates maturation of receptor tyrosine kinases. Mol. Cell. Biol. **25:**3690–3703.
35. **Tomasson, M. H., D. W. Sternberg, I. R. Williams, M. Carroll, D. Cain, J. C. Aster, R. L. Ilaria, Jr., R. A. Van Etten, and D. G. Gilliland.** 2000. Fatal myeloproliferation, induced in mice by TEL/PDGFbetaR expression, depends on PDGFβR tyrosines 579/581. J. Clin. Investig. **105:**423–432.
36. **Tsujimura, T., T. Furitsu, M. Morimoto, K. Isozaki, S. Nomura, Y. Matsuzawa, Y. Kitamura, and Y. Kanakura.** 1994. Ligand-independent activation of c-kit receptor tyrosine kinase in a murine mastocytoma cell line P-815 generated by a point mutation. Blood **83:**2619–2626.
37. **Tsujimura, T., T. Furitsu, M. Morimoto, Y. Kanayama, S. Nomura, Y. Matsuzawa, Y. Kitamura, and Y. Kanakura.** 1995. Substitution of an aspartic acid results in constitutive activation of c-kit receptor tyrosine kinase in a rat tumor mast cell line RBL-2H3. Int. Arch. Allergy Immunol. **106:**377–385.
38. **Wang, Y. Y., G. B. Zhou, T. Yin, B. Chen, J. Y. Shi, W. X. Liang, X. L. Jin, J. H. You, G. Yang, Z. X. Shen, J. Chen, S. M. Xiong, G. Q. Chen, F. Xu, Y. W. Liu, Z. Chen, and S. J. Chen.** 2005. AML1-ETO and C-KIT mutation/overexpression in t(8;21) leukemia: implication in stepwise leukemogenesis and response to Gleevec. Proc. Natl. Acad. Sci. USA **102:**1104–1109.
39. **Wu, H., U. Klingmuller, P. Besmer, and H. F. Lodish.** 1995. Interaction of the erythropoietin and stem-cell-factor receptors. Nature **377:**242–246.
40. **Yeh, H. J., G. F. Pierce, and T. F. Deuel.** 1987. Ultrastructural localization of a platelet-derived growth factor/v-sis-related protein(s) in cytoplasm and nucleus of simian sarcoma virus-transformed cells. Proc. Natl. Acad. Sci. USA **84:**2317–2321.
41. **Zuber, M. X., S. M. Strittmatter, and M. C. Fishman.** 1989. A membrane-targeting signal in the amino terminus of the neuronal protein GAP-43. Nature **341:**345–348.